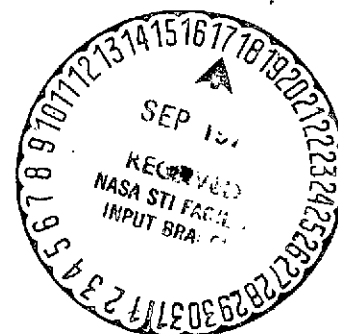# NASA TECHNICAL
MEMORANDUM

NASA TM X-64870

THE DEFINITION AND SPECIFICATION OF THE NEAR-EARTH ENVIRONMENTAL CRITERIA FOR SPACECRAFT THERMAL DESIGN

By G. A. Gary and P. D. Craven
Space Sciences Laboratory

August 1974

NASA

George C. Marshall Space Flight Center

Marshall Space Flight Center, Alabama

MSFC - Form 3190 (Rev June 1971)

1. REPORT NO. NASA TM X-64870	2. GOVERNMENT ACCESSION NO.	3. RECIPIENT'S CATALOG NO.
4. TITLE AND SUBTITLE The Definition and Specification of the Near-Earth Environmental Criteria for Spacecraft Thermal Design		5. REPORT DATE August 1974
		6. PERFORMING ORGANIZATION CODE
7. AUTHOR(S) G. A. Gary and P. D. Craven		8. PERFORMING ORGANIZATION REPORT #
9. PERFORMING ORGANIZATION NAME AND ADDRESS George C. Marshall Space Flight Center Marshall Space Flight Center, Alabama 35812		10. WORK UNIT NO.
		11. CONTRACT OR GRANT NO.
12. SPONSORING AGENCY NAME AND ADDRESS National Aeronautics and Space Administration Washington, D.C. 20546		13. TYPE OF REPORT & PERIOD COVERED Technical Memorandum
		14. SPONSORING AGENCY CODE

15. SUPPLEMENTARY NOTES

Prepared by Space Sciences Laboratory, Science and Engineering

16. ABSTRACT

Assuming the needs of the spacecraft thermal design engineer, the thermal environmental criteria are discussed, with the objective of refining the present values of the earth albedo and thermal radiation. The statistical analysis procedures which could be employed to obtain the criteria from satellite data are delineated. As an example of the program suggested, the desired parameters, displays, and methods of approach are given explicitly for albedo radiation.

17. KEY WORDS	18. DISTRIBUTION STATEMENT Unclassified - Unlimited G. A. Gary

19. SECURITY CLASSIF. (of this report) Unclassified	20. SECURITY CLASSIF. (of this page) Unclassified	21. NO. OF PAGES 66	22. PRICE NTIS

TABLE OF CONTENTS

LIST OF ILLUSTRATIONS

LIST OF ILLUSTRATIONS (Concluded)

LIST OF TABLES

THE DEFINITION AND SPECIFICATION OF THE NEAR-EARTH ENVIRONMENTAL CRITERIA FOR SPACECRAFT THERMAL DESIGN

SUMMARY

The variation of the earth's thermal and albedo radiation received by a near-earth orbiting space vehicle or space payload as a result of temporal variation of the earth-atmosphere is discussed. The time average effective value is introduced and defined as the average of the effective value of the albedo or thermal radiation affecting a thermal system in orbit. The time increment used determines the orbital segment over which the values are averaged. Time average effective values are the important values to the thermal designer. The values are independent of the spacecraft and dependent only on the character of the earth-atmosphere system. The time average effective values have a probability distribution which is dependent upon the time increment. A statistical study of current satellite data can give these probability distributions. With these distributions the thermal designer can define confidence levels on predicted temperature ranges which are compatible with engineering models for use in design, failure probabilities, and spacecraft cost estimates. Use of the distributions in environmental criteria guidelines will improve current criteria in that the guidelines will be based on satellite data and will be compatible with engineering models.

INTRODUCTION

The problem treated herein centers on the values and definitions of the time-dependent thermal environmental design parameters for a spacecraft in a near-earth orbit as employed by the thermal design engineer. Table 1 presents the current thermal environmental criteria parameters as given in Reference 1 for thermally emitted earth radiation, reflected albedo radiation, and the total direct solar radiation. The uncertainty involved in specifying the direct solar radiation impinging on a spacecraft is caused by experimental errors and not solar variation of energy output. However, the

TABLE 1. PRESENT THERMAL ENVIRONMENTAL CRITERIA [1][a]

Variation of the Time Average Effective Values About Their Global Values		
Time Increment	Albedo Variation	Earth Emitted Thermal Radiation Variation (W/m^2)
$\Delta t < 0.3$ hr	$0.30\,^{+0.30}_{-0.15}$	$237\,^{+28}_{-97}$
$0.3 < \Delta t < 3$ hr	0.30 ± 0.10	$237\,^{+24}_{-48}$
$\Delta t > 3$ hr	0.30 ± 0.05	237 ± 21

a. Solar constant = 1353 ± 13.5 W/m^2 at 1 AU

variation present in the radiation coming from the earth is a result of the numerous parameters which affect those values and which are time dependent. These time-dependent parameters, which encompass the geophysical and meteorological environments that lie below the orbit of the spacecraft, are the subject of this report.

The present criteria have several defects which can be eliminated through a judicial statistical study. The variation of the time average effective values are now, at best, an educated guess. The lack of defined confidence levels for the values makes them incompatible with engineering models used in design, failure probabilities, and spacecraft cost estimates. The variations given are altitude independent and are not a smooth function of the time increment but are step functions. The albedo and thermal infrared radiation values are not interconnected. This is unrealistic and leads to ill-defined root-mean-square procedures for the thermal design engineer. As a starting point for the discussion of a procedure for improving the criteria, the fundamentals and nomenclature will be considered.

DEFINITIONS

The concept for this report can be explained through the primary consideration of the variation of the time average effective value. The definition relating to this term will now be introduced [2].

Time Average Effective Albedo

If ds is an element of area of the earth-atmosphere[1] surface at P in Figure 1, the polar coordinates (θ_0, ϕ_0) are the zenith and azimuth angles of the incident radiation of wavelength λ upon the surface located at colatitude η and longitude east ζ, and (θ, ϕ) are the zenith and azimuth angles of a reflected ray, then the spectral radiance[2] in the direction (θ, ϕ) is given at time t by [2]:

$$N_\lambda (\zeta, \eta, t, \theta_0, \phi_0, \theta, \phi) = \frac{1}{\pi} \rho_\lambda (\zeta, \eta, t, \theta_0, \phi_0, \theta, \phi) \cos\theta \cos\theta_0 H_\lambda$$

$$(1)$$

where H_λ is the spectral irradiance[3] from the direction (θ_0, ϕ_0) in watt cm^{-2} μm^{-1} and $\rho_\lambda (\zeta, \eta, t, \theta_0, \phi_0, \theta, \phi)$ is the spectral bidirectional reflectance, i.e., the fraction of the radiation incident from the direction (θ_0, ϕ_0) which is reflected in the direction (θ, ϕ).

The total reflected radiation per unit wavelength from the element of area ds is given by the integral over the hemisphere normal to the surface,

---

1. A surface is assumed which has the properties of a combined earth surface and atmosphere.

2. Spectral radiance is the radiant energy per unit of time per unit wavelength that leaves a surface per unit solid angle and per unit projected area of that surface [3].

3. Spectral irradiance is the radiant energy per unit time per unit wavelength that is incident upon a surface per unit area [3].
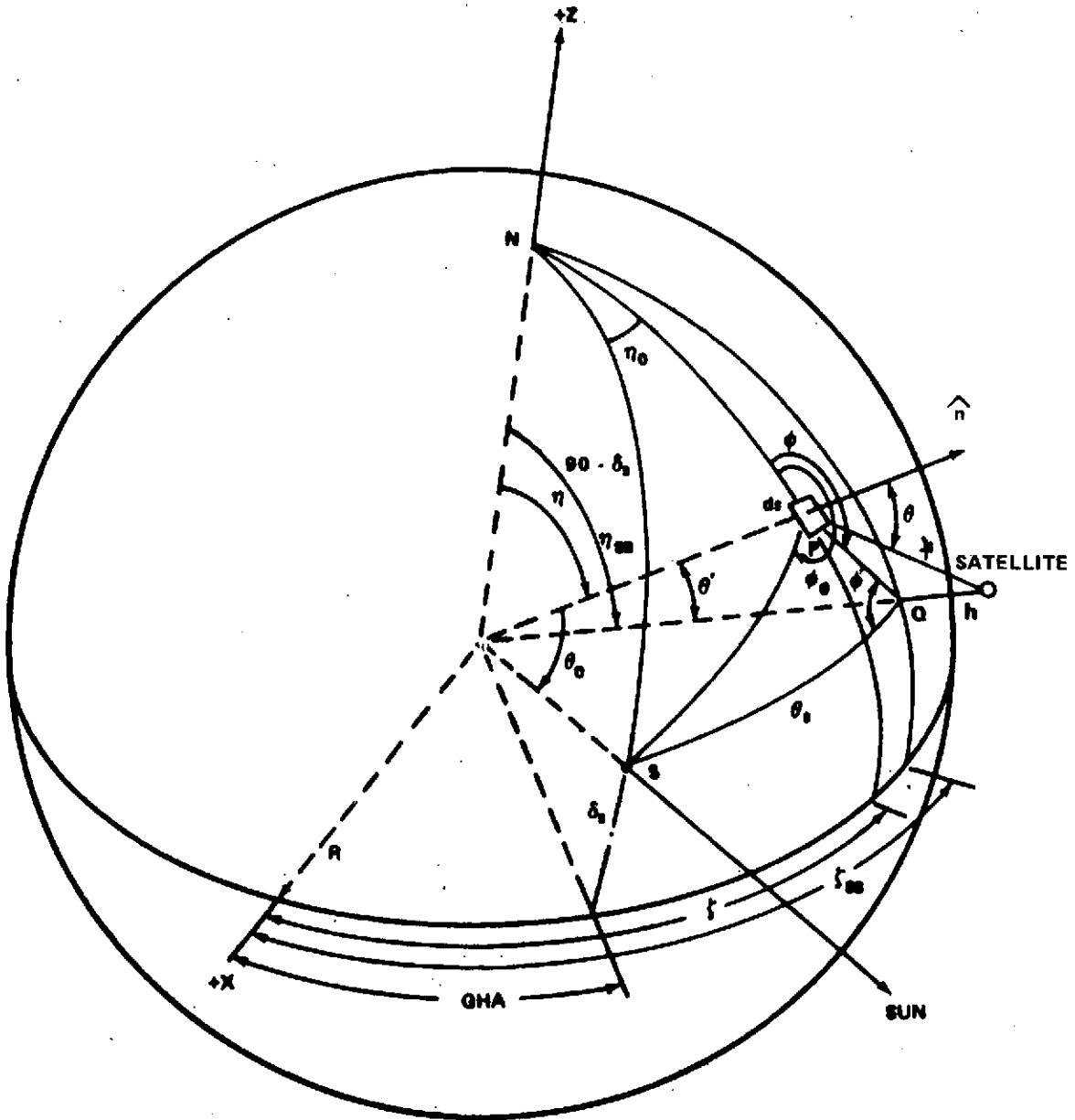
Figure 1. Geometry of the earth-atmosphere system, the sun, and the satellite.

i.e.,

$$
W^\lambda \, ds = \left[\int_{\phi=0}^{2\pi} \int_{\theta=0}^{\pi/2} N_\lambda(\zeta, \eta, t, \theta_0, \phi_0, \theta, \phi) \sin\theta \, d\theta \, d\phi \right] ds \quad . \quad (2)
$$

The spectral directional reflectance $r_\lambda(\theta_0, \phi_0, \zeta, \eta, t)$, defined as the fraction of radiation incident from direction (θ_0, ϕ_0) which is reflected, is

$$
r_\lambda(\theta_0, \phi_0, \zeta, \eta, t) = \frac{W^\lambda \, ds}{H_\lambda \cos\theta_0 \, ds}
$$

$$
= \frac{1}{\pi} \int_{\phi=0}^{2\pi} \int_{\theta=0}^{\pi/2} \rho_\lambda(\zeta, \eta, t, \theta_0, \phi_0, \theta, \phi) \cos\theta \sin\theta \, d\theta \, d\phi \quad .
$$

$$
(3)
$$

For a perfectly diffuse (Lambertian) reflectance,

$$
\rho_\lambda(\zeta, \eta, t, \theta_0, \phi_0, \theta, \phi) = \rho_\lambda(\zeta, \eta, t) \quad , \quad (4)
$$

which is independent of the incident and reflected directions. From this the following relation is obtained

$$
r_\lambda(\theta_0, \phi_0, \zeta, \eta, t) = \rho_\lambda(\zeta, \eta, t) \quad . \quad (5)
$$

Therefore, r_λ is also independent of the direction of incidence and reflection.

The average or "total" directional reflectance over a range of wavelength λ_1 and λ_2 is given by

$$r(\theta_0, \phi_0, \zeta, \eta, t) = \frac{\int_{\lambda_1}^{\lambda_2} r_\lambda(\theta_0, \phi_0, \zeta, \eta, t)\, H_\lambda\, d\lambda}{\int_{\lambda_1}^{\lambda_2} H_\lambda\, d\lambda}$$

$$= \frac{\int_{\lambda_1}^{\lambda_2} \int_{\phi=0}^{2\pi} \int_{\theta=0}^{\pi/2} \rho_\lambda(\zeta, \eta, t, \theta_0, \phi_0, \theta, \phi)\, H_\lambda \cos\theta \sin\theta\, d\theta\, d\phi\, d\lambda}{\pi \int_{\lambda_1}^{\lambda_2} H_\lambda\, d\lambda} \qquad (6)$$

The value r is also referred to as the "local" albedo when the wavelength interval covers the spectrum and a Lambertian reflectance is assumed.

The flux received by a spherical detector of radius a at an orbital height h above the earth of radius R is given by:

$$\Phi^A(\zeta_{ss}, \eta_{ss}, t, h) = \iiint N_\lambda \left[\theta_0(\zeta, \eta), \phi(\zeta, \eta), \theta(\zeta, \eta), \zeta, \eta, t\right] \Delta\Omega\, R^2 \sin\zeta\, d\lambda\, d\zeta\, d\eta \qquad (7)$$

where $R^2 \sin\zeta\, d\zeta\, d\eta$ is the reflecting surface element, $\Delta\Omega$ is the solid angle subtended by the spherical detector at the element of area, and (ζ_{ss}, η_{ss}) is the subsatellite point Q. Explicitly, (θ_0, ϕ_0) are time dependent since they are measured from the subsolar point S which is defined by the declination and Greenwich hour angle of the sun. The coordinates (θ, ϕ) and the solid angle $\Delta\Omega = \pi a^2/\rho^2$ can be found from the geocentric coordinates of the satellite and of the surface (ζ, η). The distance ρ is from ds to the spherical detector and is given by

$$\rho = \sqrt{(R+h)^2 + R^2 - 2R(R+h)\cos\theta'}$$

where θ' is defined in Figure 1.

Following the assumption that the earth has a homogeneous earth-atmosphere surface of constant Lambertian reflectance r, the flux received would be

$$\Phi^A = \iiint \Delta\Omega\, \frac{\rho_\lambda}{\pi} \cos\theta \cos\theta_0\, H_\lambda R^2 \sin\zeta\, d\zeta\, d\eta\, d\lambda \quad . \qquad (8)$$

Since ρ_λ does not depend on ζ or η, a new set of geocentric coordinates (θ', ϕ') can be used to specify the surface element depending only on the relative position of P and Q. Therefore,

$$\Phi^A = \rho \; \frac{S}{\pi} \int\int \frac{\cos\theta \, \cos\theta_0 \, R^2 \sin\theta' \, \pi a^2 \, d\theta' d\phi'}{(R + h)^2 + R^2 - 2R(R + h)\cos\theta'} \qquad . \qquad (9)$$

The total reflectivity has been used and is defined by

$$\rho = \frac{\int \rho_\lambda \, H_\lambda \, d\lambda}{\int H_\lambda \, d\lambda} \qquad .$$

The solar constant S has also been introduced,

$$S = \int_0^\infty H_\lambda \, d\lambda \qquad .$$

It is seen from Figure 1 that

$$\cos\theta_0 = \cos\theta' \cos\theta_s + \sin\theta' \sin\theta_s \cos\phi'$$

and

$$\cos\theta = \frac{(R + h)\cos\theta' - R}{\rho} \qquad .$$

Hence,

$$\Phi^A = 2a^2 \, S\rho \, R^2 \int_0^{\theta'_{max}} \int_0^\pi \frac{(\cos\theta' \cos\theta_s + \sin\theta' \sin\theta_s \cos\phi')}{[R^2 + (R + h)^2 - 2R(R + h)\cos\theta']^{3/2}} \, [(R + h)\cos\theta' - R] \sin\theta' \, d\theta' \, d\phi' \qquad ,$$

$$(10)$$

assuming the area of the earth below the detector is completely sunlit without the terminator visible where

$$\theta'_{max} \leq \frac{\pi}{2} - \theta_s \quad .$$

θ'_{max} is defined by the θ' which specifies the surface elements on the local horizon for the detector $\cos \theta'_{max} = R/(R + h)$. The integral in equation (10) is the albedo form factor for a sunlit earth.[4]

The diffuse Lambertian reflectance for the earth is the albedo used in thermal design. Hence, for a specific time t, the effective albedo for an orbiting detector would be

$$\rho_e(t) = \frac{\int \int \int \rho_\lambda(\zeta, \eta, t, \theta_0, \phi_0, \theta, \phi) \cos \theta \cos \theta_0 \, H_\lambda \sin \zeta \, d\zeta \, d\eta \, \frac{1}{\rho^2} \, d\lambda}{2S \int_0^{\theta'_{max}} \int_0^\pi \frac{(\cos \theta' \cos \theta_s + \sin \theta'_s \sin \theta_s \cos \phi) \, [(R + h) \cos \theta' - R] \sin \theta' \, d\theta' \, d\phi}{[R^2 + (R + h)^2 - 2R(R + h) \cos \theta']^{3/2}}} \qquad . \qquad (11)$$

This defines the albedo as used for the models at time t. But as the detector moves in its orbit, the effective albedo changes because of changes in (1) the surface reflectance, (2) the area seen by the detector, and (3) the relative position of the sun, surface, elements, and the detector. Hence, the term "time average effective albedo" (TAEA) is introduced and defined by

$$\overline{\rho_e(t, \Delta t)} = \int_t^{t+\Delta t} \rho_e(t') \, dt' \quad .$$

---

4. The following approximation can be used for the albedo form factor [4]:

$$\frac{2}{\pi} \int_0^{\theta'_{max}} \int_0^\pi \frac{(\cos \theta' \cos \theta_s + \sin \theta' \sin \theta_s \cos \phi')}{[R^2 + (R + h)^2 + R(R + h) \cos \theta']^{3/2}} \, [(R + h) \cos \theta' - R] \, R^2 \sin \theta' \, d\theta' \, d\phi'$$

$$= 2 \left\{ \frac{1 - \left[\frac{2h}{R} + \left(\frac{h}{R}\right)^2\right]^{1/2}}{1 + \frac{h}{R}} \right\} \left[0.84 + 0.16 \exp\left(-60 \, \frac{h}{R} \, \cos \theta_s\right)\right] \quad .$$

It is the effective albedo seen by a detector taken over a time increment Δt. The statistical variation of this quantity can be used as the working criteria to determine the variation of the radiation due to albedo.

Time Average Effective Thermal Radiation

If ds is an element of area of the earth-atmosphere surface at point P and (θ, ϕ) are the zenith and azimuthal angles of an emitted ray of wavelength λ, then the spectral radiance of the thermal emitted radiation at colatitude η and a longitude ζ is given at time t by [5]

$$N_\lambda^{IR}(\eta, \zeta, t, \theta, \phi) = \epsilon_\lambda(\theta, \phi, \eta, \zeta, t) \, N_\lambda^{BB}[T(\eta, \zeta, t)] \text{ watts/m}^2 \text{ sr}$$

(12)

where $\epsilon(\theta, \phi, \eta, \zeta, t)$ is the directional emissivity of the surface element ds. The blackbody spectral radiance is given by

$$N_\lambda^{BB} = 2c^2\tilde{h}\lambda^{-5}\left[\exp\left(\frac{hc}{\lambda kT}\right) - 1\right]^{-1}$$

(13)

where c is the speed of light, T is the temperature of the body, k is Boltzmann's constant, and $\tilde{h}$ is Planck's constant.

The energy radiated in all directions per unit area is given by the radiant emittance

$$W_\lambda^{IR}(\eta, \zeta, t) = \int_0^{2\pi} \int_0^{\pi/2} N_\lambda^{IR}(\eta, \zeta, t, \theta, \phi) \cos\theta \sin\theta \, d\theta \, d\phi \quad .$$

(14)

If the surface is Lambertian, then N_λ^{IR} is independent of θ and ϕ; hence,

$$W_\lambda^{IR}(\eta, \zeta, t) = \pi N_\lambda^{IR}(\eta, \zeta, t) \quad .$$

(15)

Assuming a blackbody earth-atmosphere system in the infrared is equivalent to assuming that the system is Lambertian in that spectral region and $\epsilon_\lambda = 1$.

The total blackbody energy radiated per unit area over the entire spectral range is given by

$$W(\eta, \zeta, t) = \int W_\lambda \, d\lambda = \int_0^\infty \frac{2\pi c^2 \tilde{h} \, d\lambda}{\lambda^5 \left[\exp\left(\frac{hc}{\lambda kT}\right) - 1 \right]} = \sigma T^4 \tag{16}$$

where $\sigma = 2\pi^5 / 15 \tilde{h}^3 k^4 c^2 = 5.729 \times 10^{-8} \, W/m^2 \, °K^4$. Hence, at time t and location (η, ζ), a temperature T defines the energy radiated. The energy radiated in the direction θ per unit solid angle per unit area is given by

$$I^{IR} = \frac{\sigma T^4}{\pi} \quad . \tag{17}$$

The thermal energy received by a spherical detector of radius a at an orbital height h above the earth of radius R is given by

$$\Phi^{IR}(\eta_{ss}, \zeta_{ss}, t) = \int\int \frac{\sigma T^4}{\pi} \cos \theta \, \Delta\Omega \, R^2 \sin \zeta \, d\zeta \, d\eta \tag{18}$$

where the integral is over the area of the earth-atmosphere surface seen by the detector and $\Delta\Omega \, (= \pi a^2 / \rho^2)$ is the solid angle subtended by the spherical detector from the element of area ds. The subsatellite earth coordinates are again (η_{ss}, ζ_{ss}). Using the geometry discussion from the albedo section,

$$\Phi^{IR}(\eta_{ss}, \zeta_{ss}, t) = 2a^2 R^2 \int_0^\pi \int_0^{\pi/2} \frac{\sigma T^4(\theta', \phi')[(h + R) \cos \theta' - R] \sin \theta' \, d\theta' d\phi'}{[R^2 + (R + h)^2 - 2R(R + h) \cos \theta]^{3/2}} \quad . \tag{19}$$

If T is independent of (θ', ϕ'), then

$$\Phi^{IR}(t) = 2\pi a^2 \sigma T^4 \left[1 - \frac{\sqrt{2Rh + h^2}}{(R + h)} \right] \quad . \tag{20}$$

For a satellite, the observed or effective temperature T is determined at a specific time t; hence,

$$\Phi^{IR}(\eta_{ss},\ \zeta_{ss},\ t,\ h) \equiv \Phi^{IR}(t) \quad . \tag{21}$$

The effective blackbody radiation per unit area is given by

$$IR(t) = \sigma T^4 = \frac{\Phi^{IR}(t)}{2\pi a^2 \left[1 - \dfrac{\sqrt{2Rh + h^2}}{(R + h)} \right]} \quad . \tag{22}$$

IR(t) defines the effective thermal emitted radiation for a model of the earth-atmosphere system at time t. As the detector moves in its orbit, the effective thermal emitted radiation changes as a result of the surface temperature and its characteristics, i.e., changes of atmospheric conditions, topography, season, and time of day. Hence, the term "time average effective thermal emitted radiation" is introduced and defined by

$$\overline{IR} = \int_{t}^{t+\Delta t} IR(t')\ dt' \quad . \tag{23}$$

It is the effective radiation seen by a detector over a time increment Δt. The probability distribution of $\overline{IR}$ as a function of Δt will be used to define the criteria in order to estimate limits on the temporal variations of $\overline{IR}$.

PARAMETERS AFFECTING THE TIME AVERAGE EFFECTIVE VALUES

Geophysical Parameters

The various parameters that influence the time average effective values fall into three categories: geophysical, meteorological, and geometrical. The geophysical parameters are those that are independent of time and refer to the characteristics which arise from the physical scattering and reflection properties and the emissivities of the earth's surface and atmosphere. A detailed

discussion of these quantities is beyond the range of this report; however, a general summary for albedo is given in Table 2 [6] and Figure 2. The albedo of clouds covers a range from 0.10 to 0.80, land features cover a range from 0.05 to 0.45 except for snow- and ice-covered areas, and water covers a range of 0.02 to 0.20. The bidirectional reflectance from the earth surfaces and clouds could be obtained. However, the scattering of a Rayleigh atmosphere with aerosols presents a different picture. Snoddy concluded, "Due to the many variables and unknown factors, it is doubtful that a complete theoretical model for the reflected and scattered radiation from a planet and its atmosphere will be formulated in the near future" [7]. The effect of a Rayleigh atmosphere without aerosols can be inferred from the fact that above the subsolar point a homogeneous earth with $\rho = 0$ will have an effective albedo due to a Rayleigh atmosphere of about 0.08 [7]. Meteorological effects would drastically change this simple geophysical model.

The geophysical factors that influence the emitted thermal radiation vary, depending on surface conditions. The emission properties are a function of the surface temperature, e.g., desert, ocean, and polar region. At the atmospheric transmission region of 11 μm the following brightness temperatures were obtained from Nimbus 4 [8]:

Sahara Desert	321°K (102°F)
Mid-Latitude Ocean	280°K (44°F)
Antarctic	198°K (-103°F)

This illustrates the temperature variation over the earth.

The water content in the air changes the thermal emission of the atmosphere due to the absorption bands (e.g., H_2O). The various absorption and emission bands in the atmosphere complicate modeling by a simple geophysical atmosphere in the thermal region. As an example of the brightness temperature of the atmosphere, the CO_2 band at 15 μm emits at 215°K (-76°F). At such a temperature, the atmosphere is warmer than the antarctic surface temperature given previously. The total effective temperature is dependent on both the atmosphere and surface.

Meteorological Parameters

The meteorological parameters affecting the time average effective albedo and thermal emitted radiation are a function of time and location on the earth. Because the nature of the atmosphere is continuously changing, weather

TABLE 2. SUMMARY OF REFLECTANCE DATA FOR EARTH SURFACE
FEATURES AND CLOUDS [6]

Reflecting Surface	Magnitude and Other Spectral Characteristics	Angular Distribution of Reflectance	Total Reflectance
Soils and Rocks	Increases to 1μm Decreases above 2μm	Backscattering and forward scattering Sand has large forward scattering Loam has small forward scattering	5 to 45 percent Moisture decreases reflectance by 5 to 20 percent Smooth surfaces have higher reflectance Diurnal variation Maximum reflectance for small sun angles
Vegetation	Small below 0.5μm A small maximum bump at 0.5 to 0.55μm Chlorophyll absorption at 0.68μm Sharp increase at 0.7μm Decrease above 2μm Depends on growing season	Backscattering Small forward scattering	5 to 25 percent Diurnal effects Maximum reflectance for small angles Marked annual variation
Water Basins	Maximum at 0.5 to 0.7μm Depends on turbidity and waves	Large back and forward scattering	5 to 20 percent Diurnal variation Maximum for small sun angles depends on turbidity and waves

TABLE 2. (Concluded)

| Reflecting Surface	Magnitude and Other Spectral Characteristics	Angular Distribution of Reflectance	Total Reflectance
Snow and Ice	Decreases slightly with increasing wavelength Large variability depends on purity, wetness, and physical condition	Diffuse component plus mirror component Mirror component increases with increasing angle of incidence	Variable 25 to 80 percent 84 percent in Antarctic 74 percent in Ross Sea ice 30 to 40 percent in White Sea ice
Clouds	Constant from 0.2 μm to about 0.8 μm Decreases with wavelength above 0.8 μm, showing water vapor absorption bands	Pronounced forward scattering with small backscattering Minimum for scattering angles of 80 to 120 deg Fogbow for scattering angle of 143 deg	10 to 80 percent Varies with cloud type, cloud thickness, and type of underlying surface
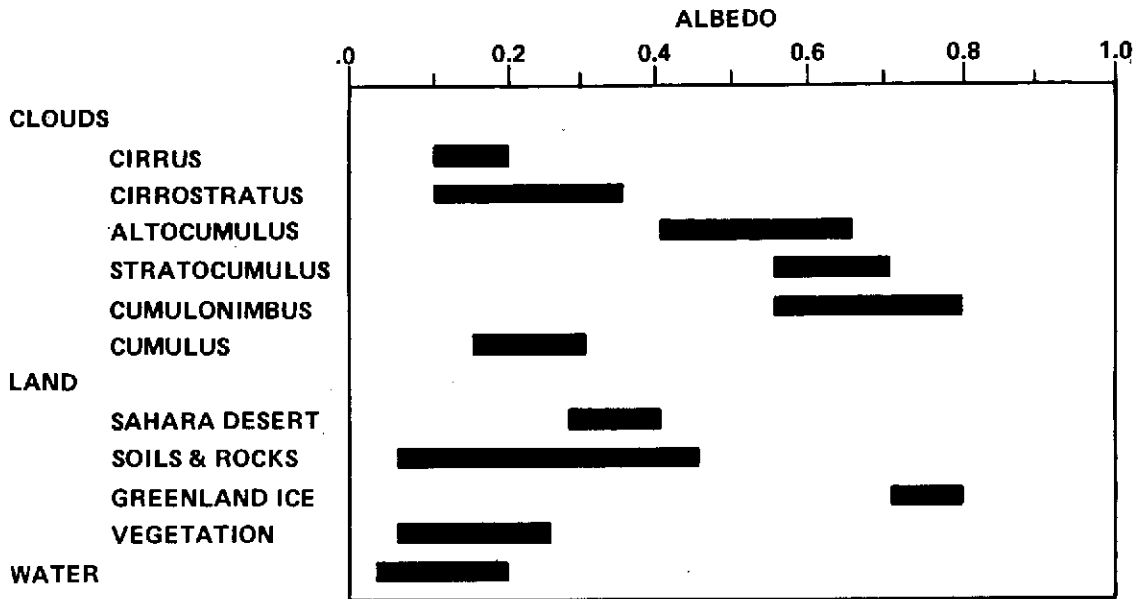
Figure 2. Local albedo variation [9, 10].

is highly variable and depends upon the temporal and spatial position over the earth. At any particular time the average cloudiness for the whole earth is between 50 and 60 percent.

The local albedo should experience a diurnal variation as a result of the diurnal variation of temperature and sun angle for a particular location. The local albedo increases as the solar zenith angle decreases. The diurnal variation of the albedo observed with Tiros 4 low resolution sensors is shown in Figure 3 [8].

From climatological consideration, seasonal variations of albedo are to be expected. Figure 4 presents the seasonal variations of albedo as determined from the 0.55 to 0.75 μm data from Tiros 7 [8]. Both sets of data were adjusted to give a mean quasi-global albedo of 32.2 The seasonal variation is ±0.05 from the global average.

The latitudinal variation of the albedo is shown in Figure 5 [11]. These data were obtained from OSO-II by treating thermal control coatings as radiometers. The values were obtained during the period March 4-8, 1964. All 643 data points lie between 33°N and 33°S latitude and are evenly distributed over all longitudes with the exception of the region between 40° W and 80°W. The OSO-I data and London' s (1957) latitudinal averages are also shown. Though
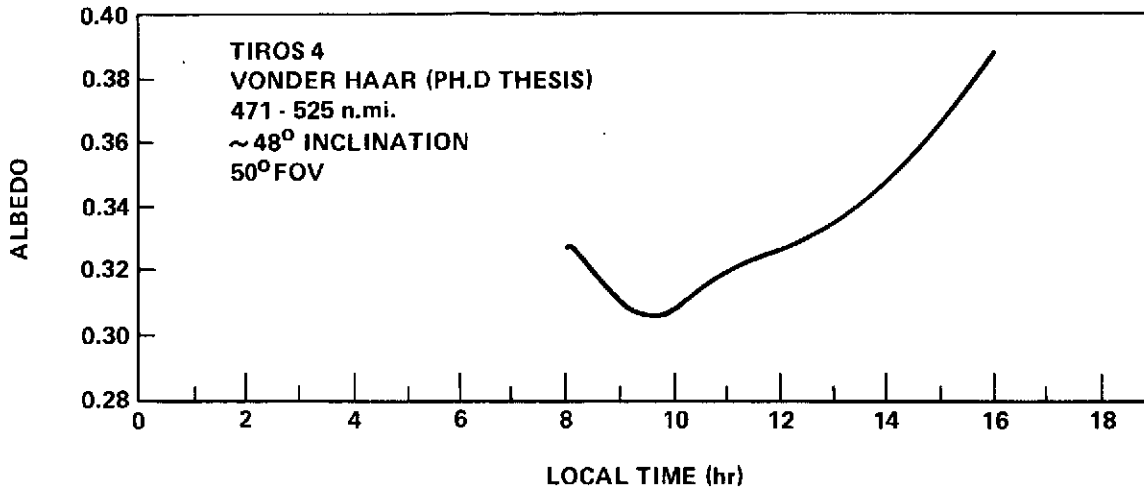
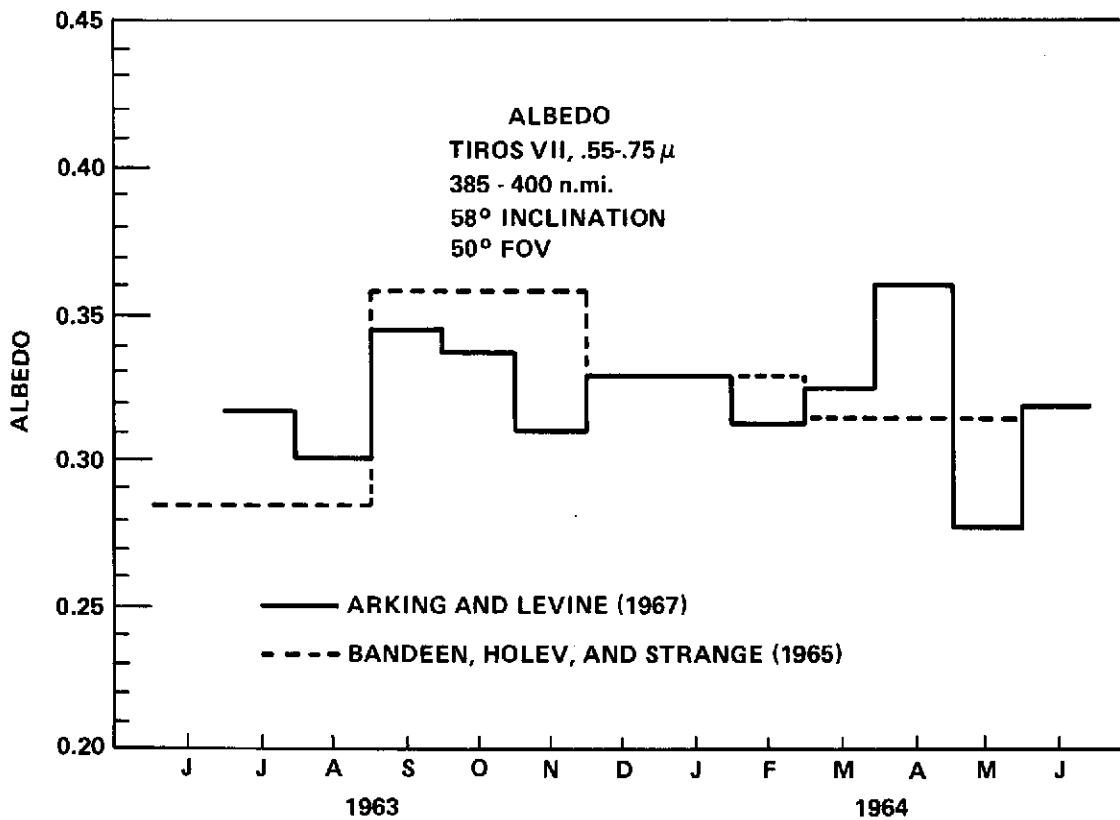Figure 3. Diurnal variation of planetary albedo [8].
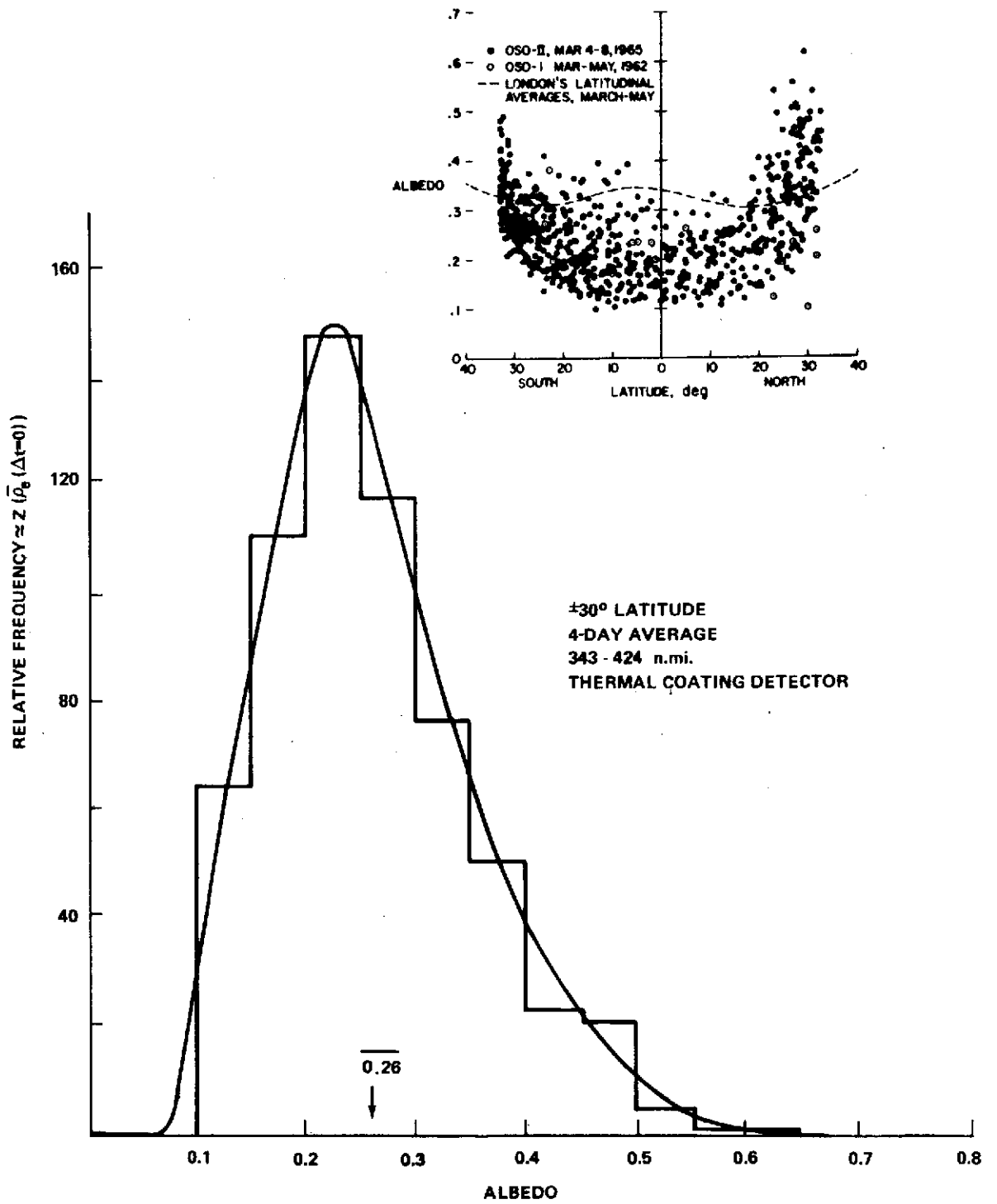

Figure 4. Seasonal variation of albedo [8].

Figure 5. Frequency distribution of the albedo from
OSO-II data [11].

the data are limited, they do indicate the global latitudinal variation resulting in part from the decreasing solar elevation angle, snow and ice cover near the poles, and increased cloud cover associated with large-scale weather activity. A probability distribution function Z of the albedo for these data is also plotted in Figure 5. The distribution covers a selected temporal and spatial region for the earth. A smooth curve through the histogram indicates the probability, but, because of the difficulty of reading the data from the latitudinal figure, this curve only represents the trend. This is exemplified by the fact that the authors obtain an average albedo of 0.26, while the investigators report an average of 0.28. The albedo measurements range from 0.10 to 0.62. The global average was 0.29 when corrected.

A representative variation of the albedo as seen by a detector is shown in Figure 6. These data of April 11, 1965, were obtained by Linton [12] using thermal data from Pegasus I. The first half of the orbit shown has no cloud formation associated with it, and the albedo recorded is that of the surface features and the effects of a Rayleigh atmosphere. The central peak at longitude 80 deg corresponds to a cloud mass.

The data from April 11, 1965; May 8, 1965; and March 20, 1965, were combined to form the probability distribution, also shown in Figure 6. This random sampling does agree in the gross feature with Figure 5 however bad the statistical sampling.

The spatial variation over the globe is shown in Figure 7 for a 15-day period and was obtained by averaging the Nimbus II data over a grid field of 5 by 5 deg of longitude and latitude at the equator and 5 by 2.5 deg at 60 deg latitude [13]. The albedo of the earth system between 40°S and 40°N during the period May 16-31, 1966, is shown for a partial swath around the earth. An albedo distribution for the swath around the earth was generated as shown. Raschke [13] presents the reflected solar radiation and the emitted infrared radiation over the entire globe from the Nimbus II meteorological satellite during the period May 16 to July 28, 1966. In general, the albedo of the polar cap is in the range from 0.60 to 0.90. Toward the equator the albedo decreases rapidly with decreasing cloudiness, showing minima of less than 0.20. The Sahara and Arabian deserts have albedo of more than 0.30 to 0.35. The global albedo was from 0.291 to 0.306.

An Apollo 8 photograph of the Western Hemisphere shows the striking variation of albedo over geographic regions (Fig. 8). Salient global cloud features can be obtained from Reference 14, which is a photographic summary of the earth's cloud cover for the year 1967.

18
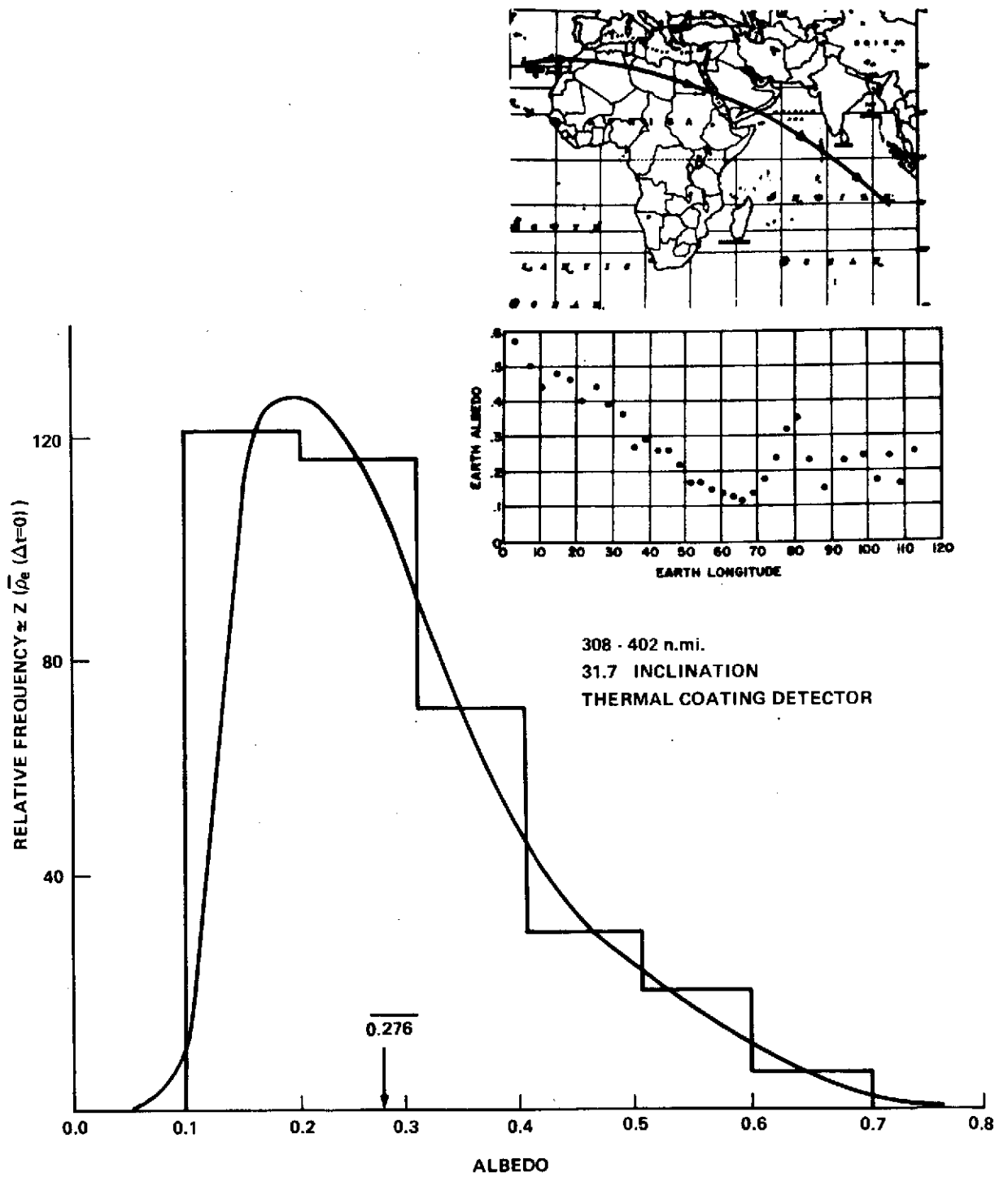
Figure 6.   Frequency distribution of the albedo from
Pegasus I orbital data [12].
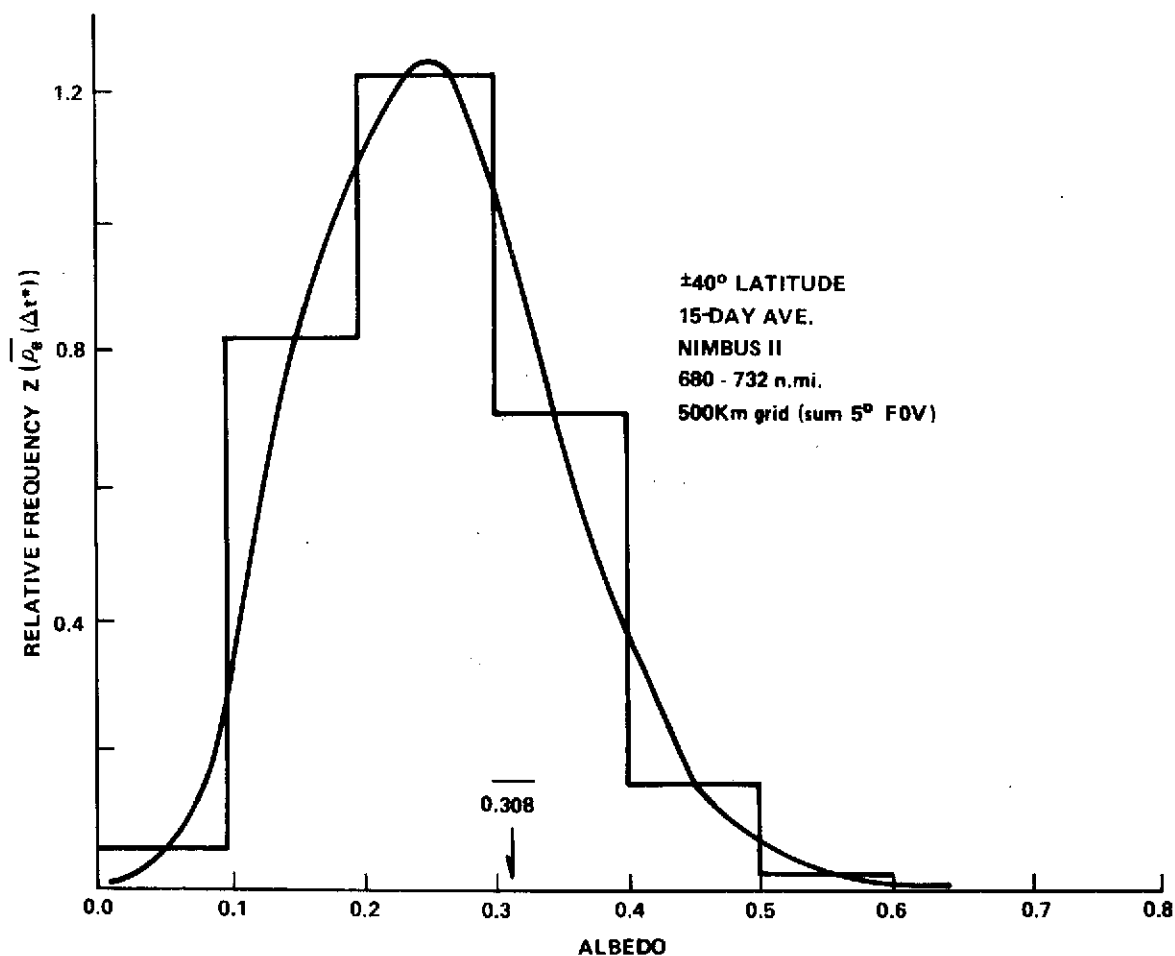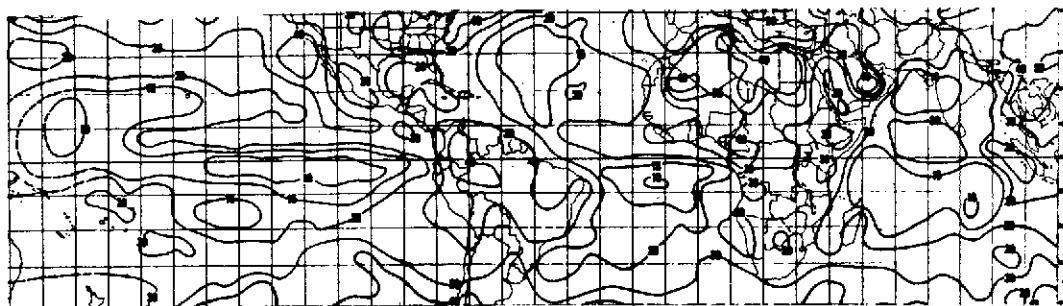
Figure 7.   Frequency distribution of the albedo from
Nimbus II between +40° N and -40° S during
the period May 16-31, 1966 [13].

Figure 8. Apollo 8 photograph of the Western Hemisphere.

The diurnal variation of the thermal emission tends to peak in the early morning and decrease through the remainder of the day [6]. The diurnal variation on a global average is ±28 W/m². For a temperature change from 273°K (32°F) to 288°K (59°F), the emission increases 76 W/m² from 318 W/m².

The mean annual and seasonal variation of the emitted infrared radiation of the earth-atmosphere system observed from the first generation meteorological satellites is given by Vonder Haar [6]:

Thermal Emitted Radiation (W/m^2)

	Global	Northern Hemisphere	Southern Hemisphere
Dec.-Feb.	223	223	230
Mar.-May	230	230	223
June-Aug.	230	237	223
Sept.-Nov.	237	237	237
Annual	230	230	230

The variation with latitude of the thermal radiation is shown in Figure 9 for a time span from June through August. These data were obtained from Tiros VII in 1963. The thermal emitted radiation is lower at the poles. The variation of the absolute magnitude at most latitudes is very small. The largest seasonal differences occur in the polar regions and are about ± 70 W/m^2 [6].

To illustrate the variation of the thermal radiation seen by a detector, OSO-I and OSO-II data were used to derive a representative distribution (Fig. 10). The peak frequency is 330 W/m^2 with sideband widths of +70 and -90.

Since the thermal radiation is correlated to the albedo through the heat balance equation, a general correlation is expected between the effective values. From Tiros VII data a correlation between the 8- to 12-μm channel and the 0.55- to 0.75-μm channel has been obtained:

$$\frac{\Delta \text{ albedo channel}}{\Delta \text{ IR channel}} = 0.0039 \ ,$$

where Δ indicates an incremental change in value. The data shown in Figure 11 were obtained by using the longitudinal maps of Bandeen [2]. The data given
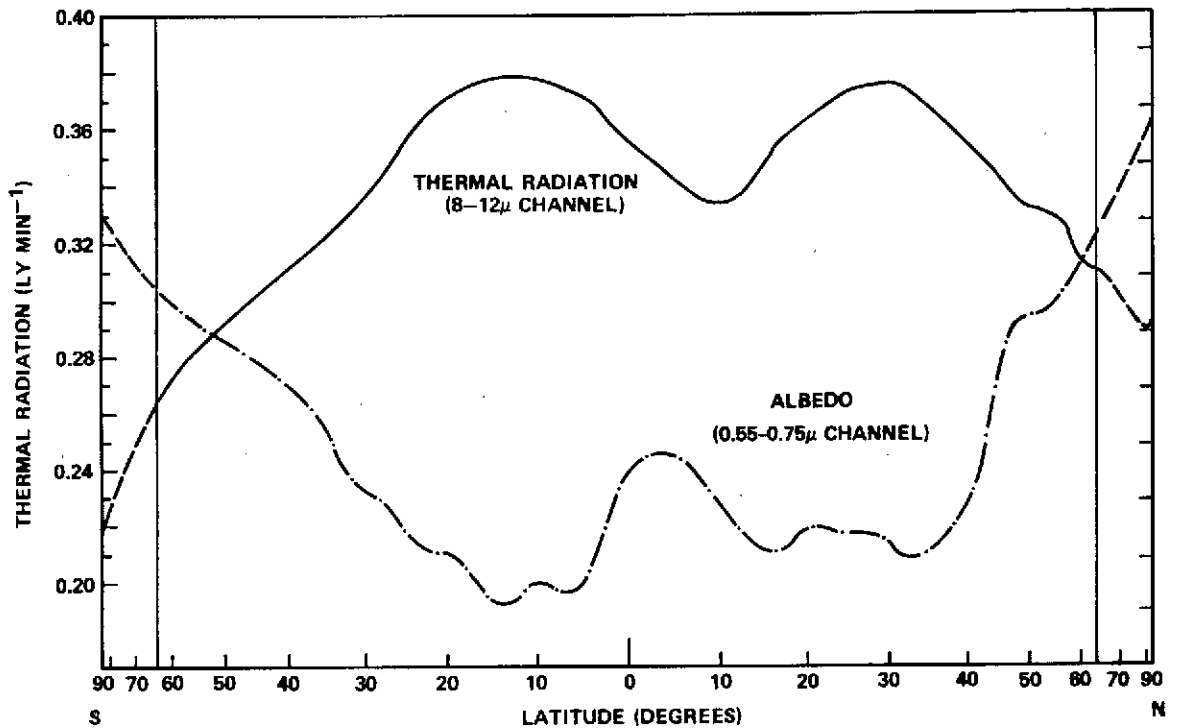
Figure 9. Tiros VII thermal and albedo radiation latitude
data for June-August 1963 [2].

in Figure 7 were transformed into a distribution of thermal emitted radiation
using the albedo and IR relationship and the following empirical formula:

Thermal Emitted Radiation = 237 - 0.0039 (albedo -0.308)   .

The results of this transformation are shown in Figure 12. The distribution
about the mean, 237 W/m^2, is shown.

The spectral distribution for the reflected albedo and thermal emitted
radiation is shown in Figure 13. The meteorological effects change the spectral
characteristics; however, the bounds indicated in the figure are representative
of the fluctuation.

Geometrical Parameters

The geometrical parameters are derived from the relative locations of
the sun, earth, and detector. These give the height of the detector, the angles
for the bidirectional reflectance, and the various solid angles.
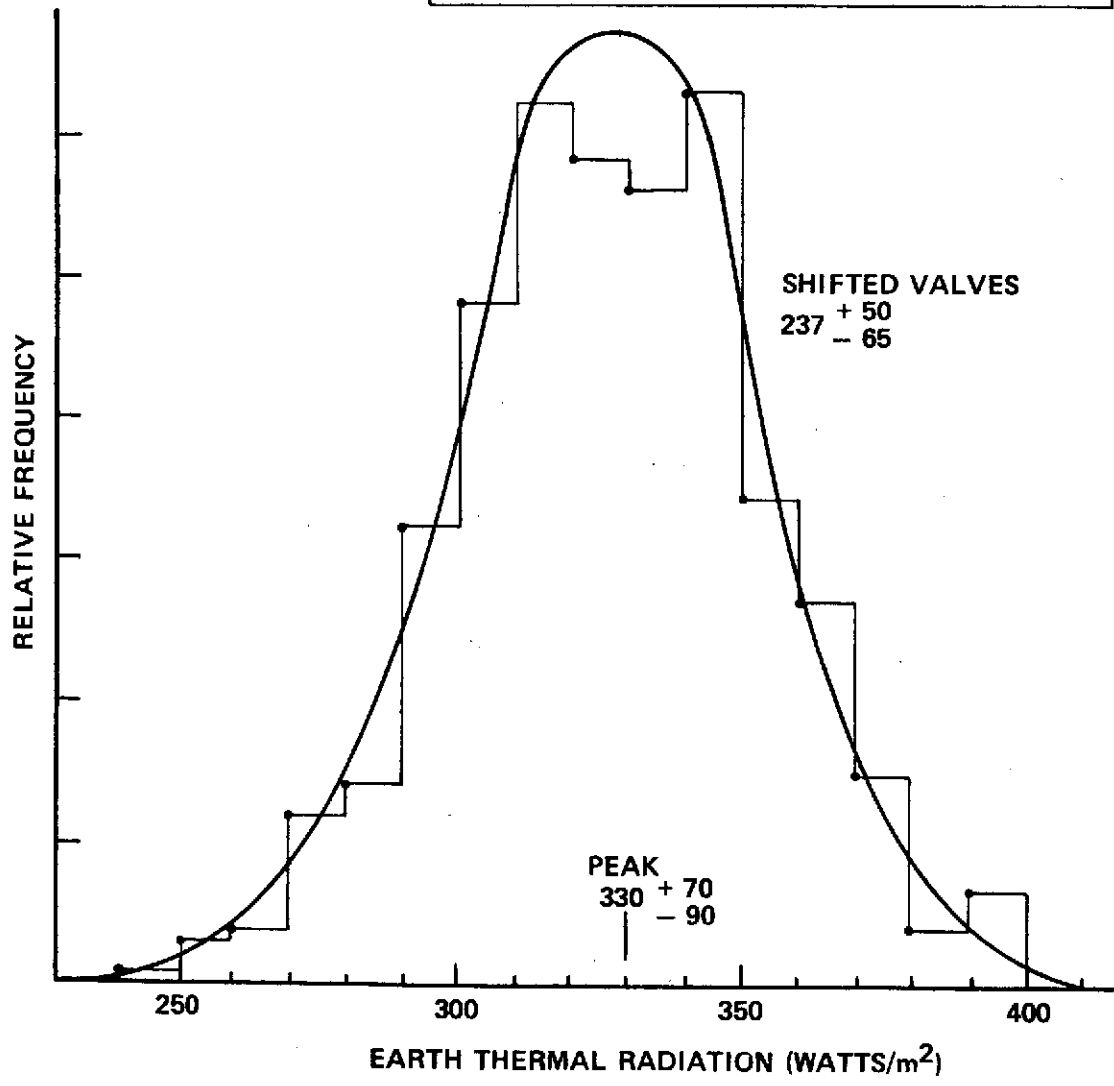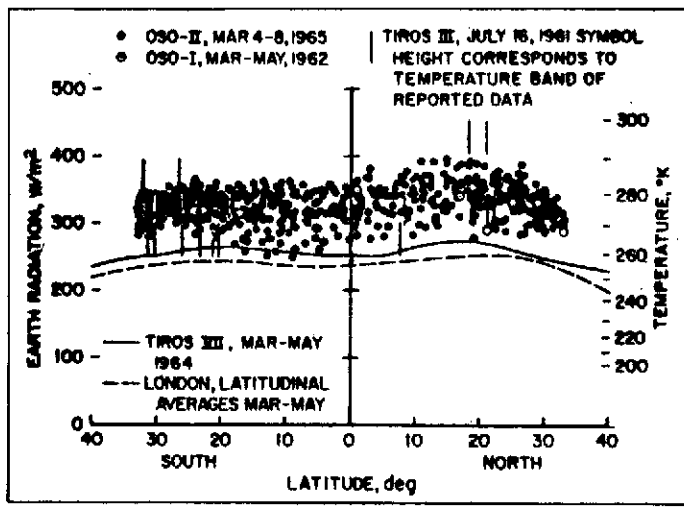
Figure 10. OSO–I and OSO–II thermal distribution function [11].
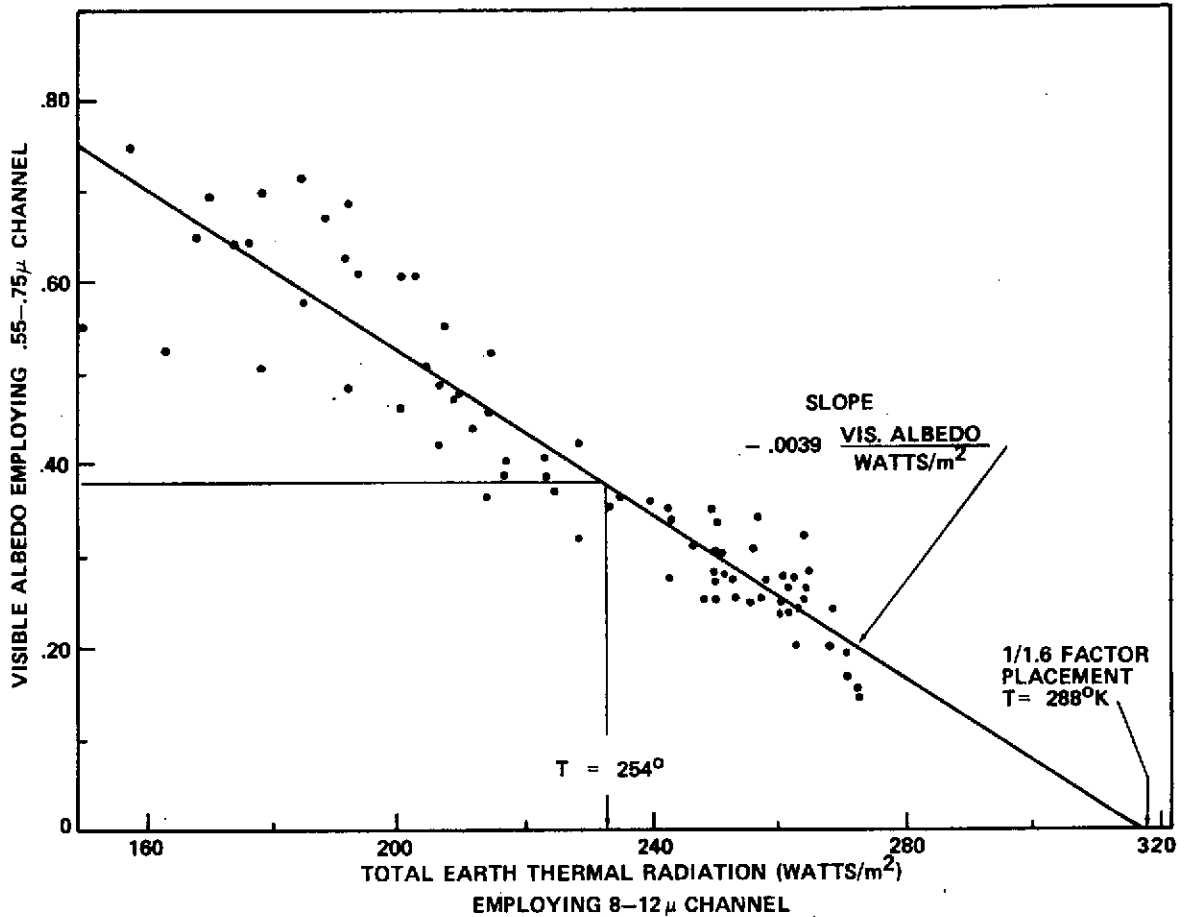
Figure 11. Tiros VII albedo-thermal radiation correlation.

The area of the earth seen from a height h is given by

$$\left(\frac{\Delta\Omega}{4\pi}\right) \ 4\pi R^2 \ = \ 2\pi\,(1 \ - \ \cos\,\theta') \ R^2 \ \simeq \ 2\pi\left(\frac{\theta'}{2}\right)^2 R^2 \ = \ \pi\,(\theta'\,R)^2 \tag{24}$$

where $\Delta\Omega$ is the solid angle of the area as viewed from the center of the earth. If β_{max} is the angle from the normal to the local horizon where $\theta' = \theta'_{max}$ (Fig. 14), then

$$\beta_{max} \ = \ \frac{\pi}{2} \ - \ \theta'_{max} \ = \ \frac{\pi}{2} \ - \ \cos^{-1}\left(\frac{R}{R \ + \ h}\right) \ . \tag{25}$$

25

EMPIRICAL EQUATION

$$\overline{IR} = 237 - 0.0039\,(A - 0.308)$$

RELATIVE FREQUENCY

EARTH THERMAL RADIATION (WATTS/m^2)

$-237\,^{+\,63}_{-\,37}$
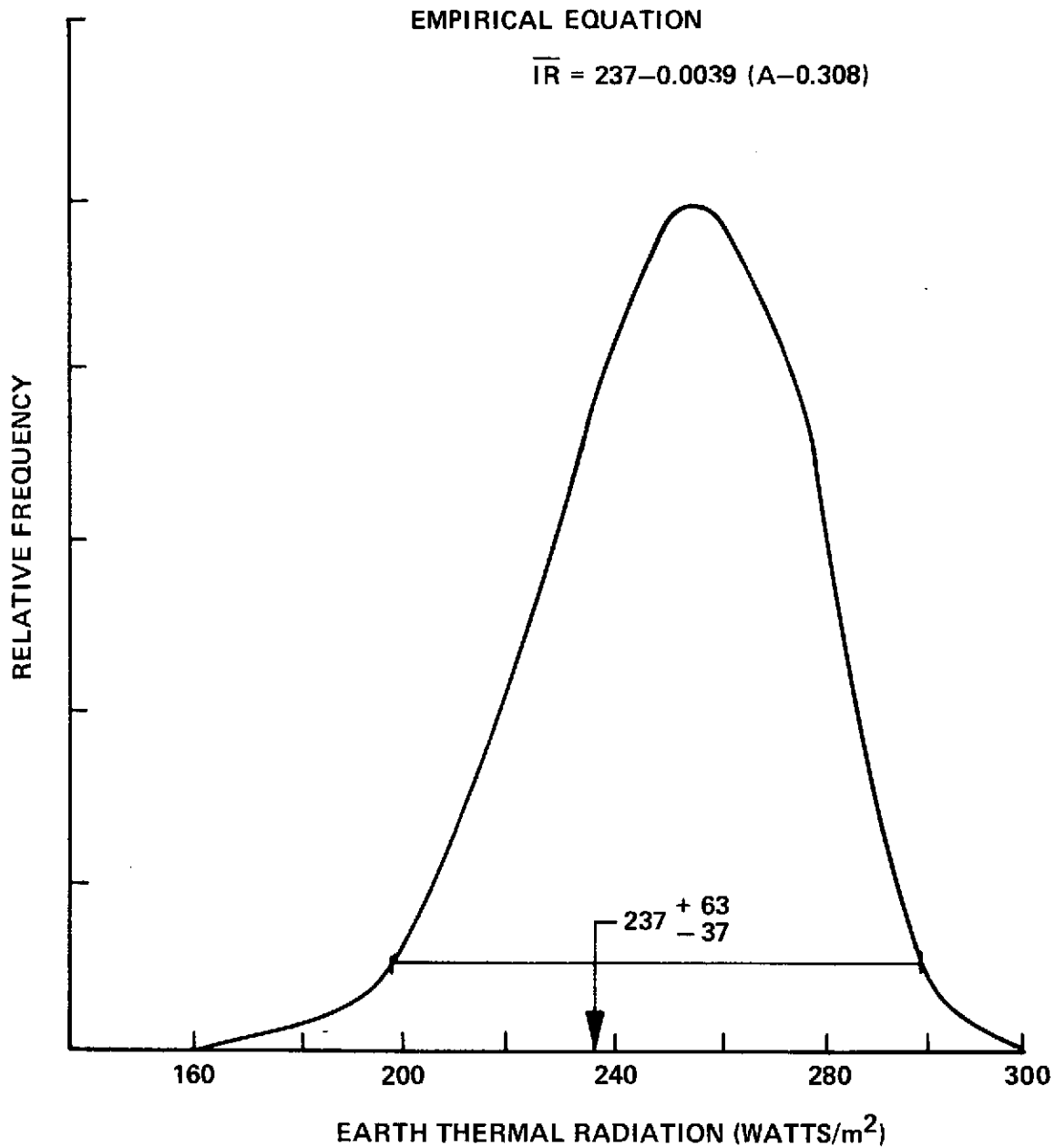
Figure 12. Empirical transformation of Nimbus II albedo data to obtain a thermal distribution function.

For a 435-km orbit, θ_{max} = 19.1 deg and β_{max} = 70.9 deg. The effect of varying β keeping h constant is examined in Table 3 and Figure 15. For a Lambertian earth, halving the solid angle of the field of view should half the radiation received by a detector. If the solid angle is halved and the above
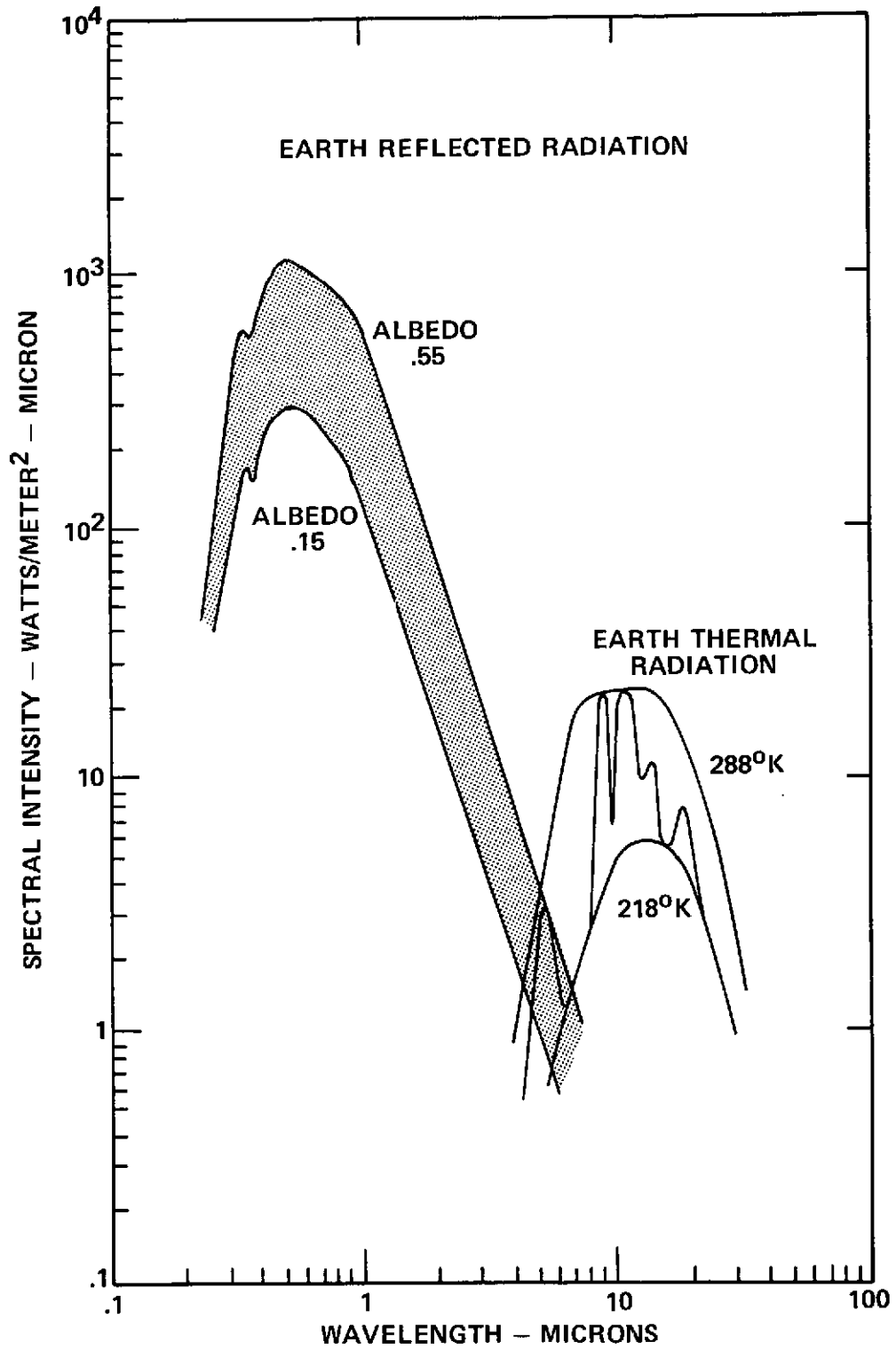
Figure 13. Spectral radiance functions for the albedo and thermal radiation emerging from the earth-atmosphere surface.
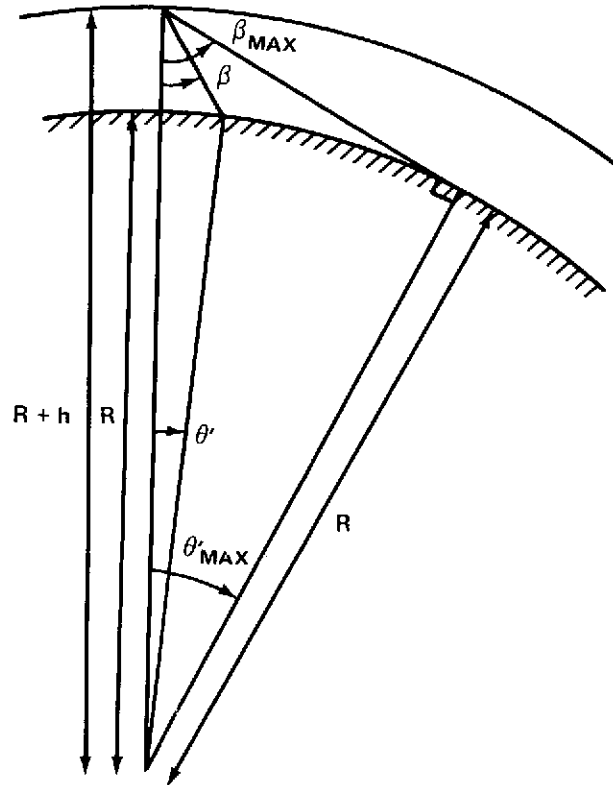
Figure 14. Geometry to define β_{max}, β, θ, and θ'_{max}.

TABLE 3. VIEWING ANGLES FOR h = 435 km

	θ'_{max} (deg)	$R\theta'_{max}$ (km)
β_{max} = 70.9 deg	19.1	2445
0.75 β_{max} = 53.4 deg	4.8	615
0.707 β_{max} = 50.0 deg	4.4	565
0.50 β_{max} = 35.4 deg	2.5	324
0.25 β_{max} = 17.7 deg	1.1	140
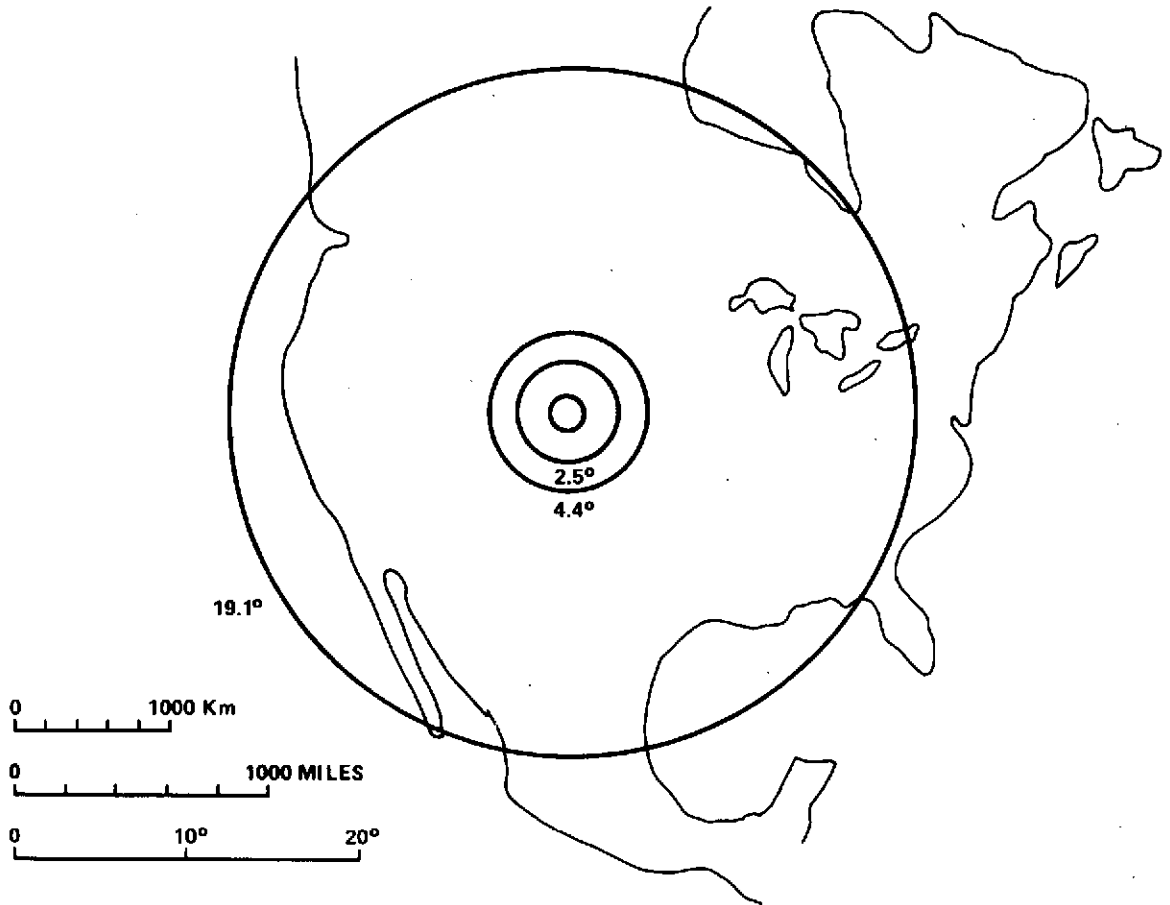
Figure 15. Effects of $\theta'(\beta, h)$ on surface area.

approximation is used, then it is seen that half of the radiation $(\beta_{max}/\sqrt{2})$ is coming from an area with a radius of 565 km about the subsatellite point. However, an area of radius 2445 km influences the total effective albedo.

To approximate the maximum rate of change the effective albedo can obtain through geometry, one assumes that the albedo ρ_e changes from 0 to 1 as the detector at height h moves $2\theta'_{max}$ (Fig. 16).

Since the period of the orbit is

$$P = 2\pi \sqrt{\frac{(R + h)^3}{GM}} \quad , \tag{26}$$
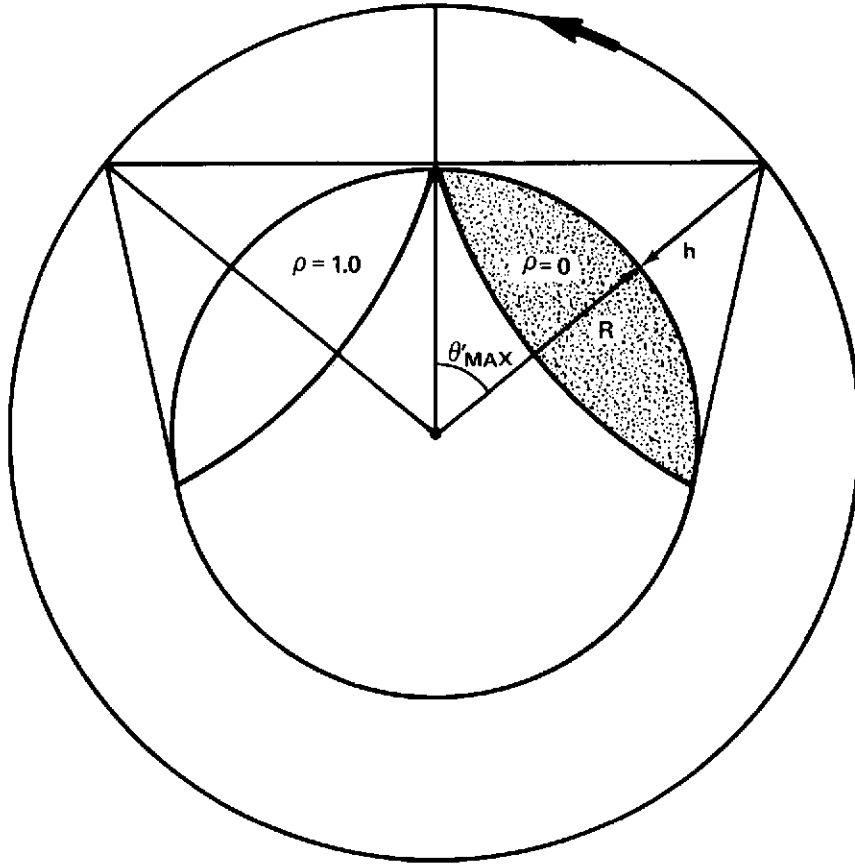
Figure 16. The case of the albedo changing from $\rho_e = 0$ to $\rho_e = 1$.

the rate is

$$\frac{d\rho}{dt} = \Delta\rho \left[\left(\frac{2\theta'_{max}}{2\pi} \right) 2\pi \sqrt{\frac{(R + h)^3}{GM}} \right]^{-1} \tag{27}$$

where $\cos\theta'_{max} = R/R + h$. For $h = 435$ km $(235$ n. mi.$)$, $P = 93.6$ and $d\rho/dt \simeq 1.7 \times 10^{-3}/\text{sec}$.

Increasing the height will decrease the rate by increasing the time for the detector to move $2\theta'_{max} \xrightarrow[h\to\infty]{} \pi$. The area below the detector also becomes larger and the average effective albedo is influenced by a larger area. But, as h increases, the influence of the albedo compared to the direct solar thermal input decreases. Figure 17 presents the view factor, defined by $\Phi^A_{received}/\rho S\pi a^2$ for a sphere of projected area πa^2 and a Lambertian earth

30
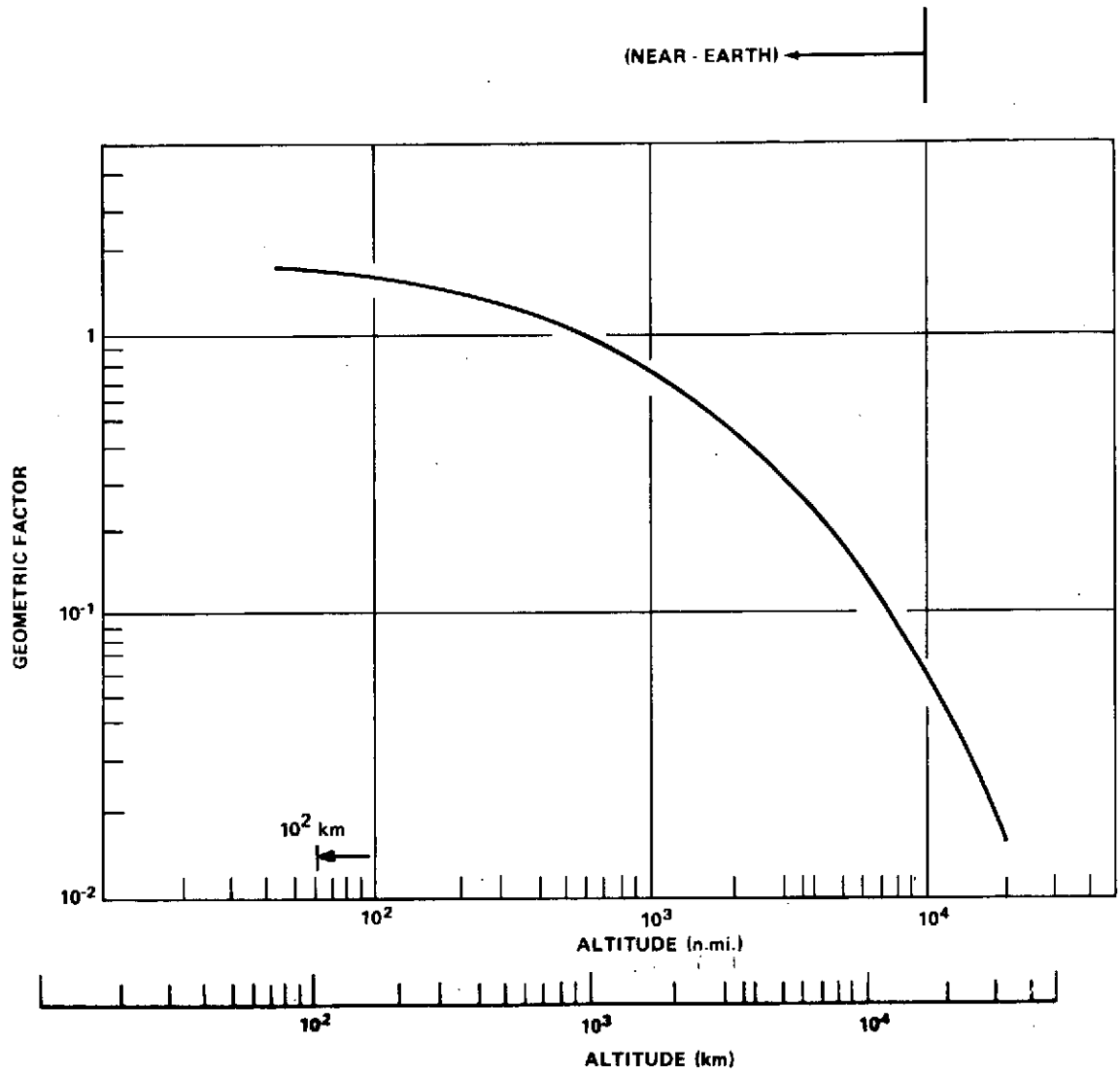
Figure 17. The geometric view factor $(\Phi/\pi a^2 S\rho)$ for reflected
Lambertian radiation incident on a sphere versus altitude
for a solar zenith angle of zero [15].

as a function of height [see equation (10)]. Similarly, the view factor for the
thermal radiation is defined as $\Phi_{received}^{IR}/I_t\pi a^2$ where I_t is the energy
radiated per unit area at the earth-atmosphere surface.

At 10^4 km the albedo input even for $\rho = 1$ is less than 0.10. The value 10^4 km for h will be used to define the limit height for near-earth orbits.

DERIVATIONS OF THE TIME AVERAGE EFFECTIVE ALBEDO

The time average effective albedo depends on the geophysical, meteorological, and geometrical inputs for the temporal and spatial regions under consideration. Therefore, the TAEA,

$$\overline{\rho_e(t,\ \Delta t)} = \int_t^{\Delta t} \rho_e(t')\ dt'\quad,\tag{28}$$

fluctuates between certain limits depending on Δt, the orbit, and the earth-atmosphere system in the swath of the detector. The distribution of the time average effective albedo for given parameters (such as the orbital height) versus the time increment is needed in thermal design. Several procedures for determining the TAEA will be discussed. The mean, 1σ, 2σ, and 3σ values (σ is the standard deviation) are the quantities needed by the thermal design engineer because these quantities characterize the probability distribution. The 1σ, 2σ, and 3σ symbols indicate that the proportion of the values found within the interval of the mean plus and minus $n\sigma$ (n = 1, 2, 3) are 68.3, 95.4 and 99.7 percent, respectively. This does not mean that the probability distribution of TAEA $Z\overline{[\rho_e(t,\ \Delta t)]}$ is a standard normal distribution function.

Theoretical Distribution

The following is a theoretical derivation of the probability function for the time average effective albedo. Physically, the TAEA cannot have values greater than 1.0 or less than 0. The physical distribution is required to have a 0 probability at 0 and 1. The restricted range requirement does not allow a normal distribution function to approximate $Z(\overline{\rho_e})$ directly. Hence, a transformation is introduced. The transformation of $\overline{\rho_e(\Delta t)}$ to x by

$$x = \frac{\overline{\rho_e(\Delta t)} - 0.30}{\overline{\rho_e(\Delta t)}\ [1 - \overline{\rho_e(\Delta t)}]}\tag{29}$$

gives values at $\overline{\rho_e(\Lambda t)} = 0.30$ of x = 0.0, at $\overline{\rho_e(\Delta t)} \simeq 1$ an x value of $+\infty$, and at $\overline{\rho_e(\Delta t)} \simeq 0$ an x value of $-\infty$. Hence, one can reconcile the normal distribution approximation using the parameter x. For the normal distribution, the probability of finding an albedo such that $a \le x \le b$ is given by

$$P(a \le x \le b) = \int_a^b \frac{1}{\sqrt{2\pi}\sigma} e^{-(x-\mu)^2/2\sigma^2} dx \qquad (30)$$

where σ^2 is the variance (and σ is the standard deviation),

$$\sigma^2 = \int_{-\infty}^{+\infty} (x - \mu)^2 \frac{1}{\sqrt{2\pi}\sigma} e^{-(x-\mu)^2/2\sigma^2} dx \quad,$$

μ is the mean,

$$\mu = \int_{-\infty}^{+\infty} x \frac{1}{\sqrt{2\pi}\sigma} e^{-(x-\mu)^2/2\sigma^2} dx \quad,$$

and

$$P(-\infty \le x \le \infty) = 1 \quad.$$

The integrand of $P(a \le x \le b)$ is the probability function $Z(x)$. Figure 18 shows the normal distribution function Z and the corresponding values of $\overline{\rho_e(\Delta t)}$ under the transformation. In the above case, $\mu = 0$ and $\sigma = 1$. Using the inverse transformation

$$\overline{\rho_e(\Delta t)} = \frac{x - 1 + \sqrt{(x-1)^2 + 1.2x}}{2x} \qquad (31)$$

the confidence values in Table 4 are obtained. The probability distribution function $Z[\overline{\rho_e(\Delta t)}]$ in terms of $\overline{\rho_e(\Delta t)}$ is shown in Figure 19 along with the position of the 1σ, 2σ, and 3σ values.
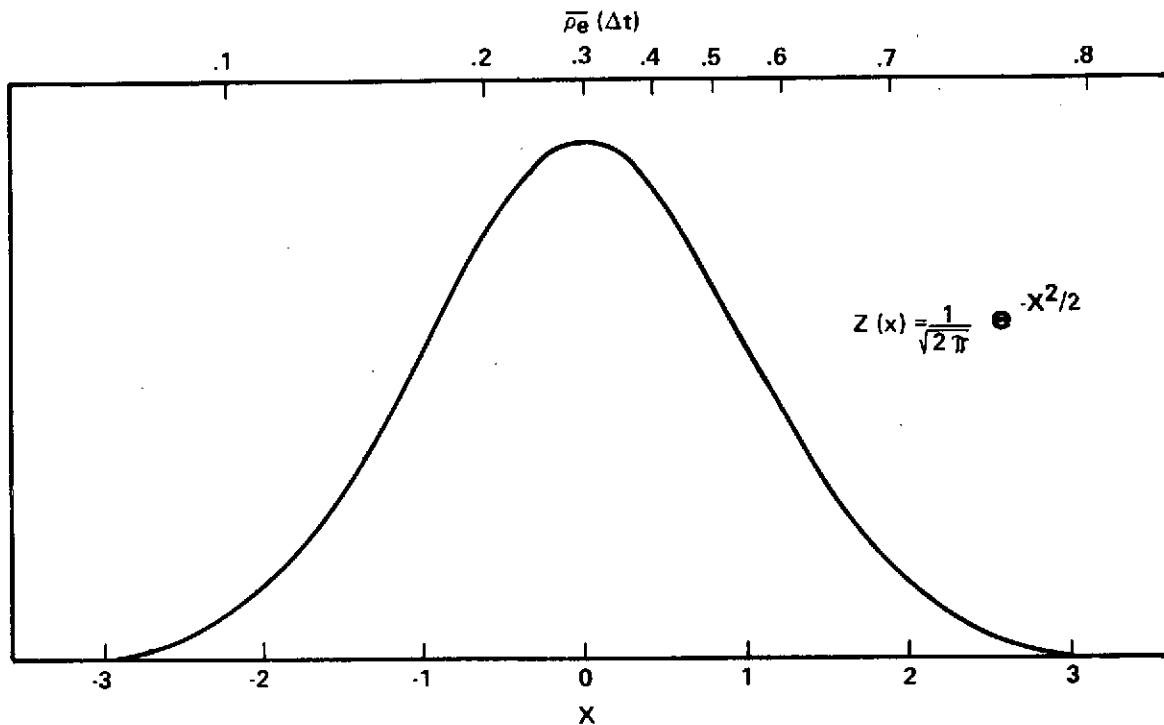
Figure 18. Normal (gaussian) probability function showing the corresponding $\bar{\rho}_e$ locations under the transformation.

TABLE 4. CONFIDENCE VALUES IN TERMS OF x AND $\overline{\rho_e(\Delta t)}$

x	$\overline{\rho_e}$ (Minimum)	$\overline{\rho_e}$ (Maximum)	Probability (%)
1	0.163	0.548	68.3
2	0.108	0.711	95.4
3	0.080	0.793	99.8

Because of the similarity of the OSO-II and Pegasus I data in Figures 5 and 6 to the $Z(\overline{\rho_e})$ just derived, this function of $Z[\overline{\rho_e(\Delta t)}]$ shall be assumed for the moment to describe the distribution of $\overline{\rho_e(\Delta t)}$ at $\Delta t = 0$. Furthermore, it is assumed that at a time increment $\Delta t = 2$ hr, the function $Z(\overline{\rho_e})$ is normal with $3\sigma = 0.10$, and as $\Delta t \rightarrow \infty$ it becomes a normal function with $3\sigma = 0.05$. A 3σ of 0.05 is similar to actual seasonal variation. The points
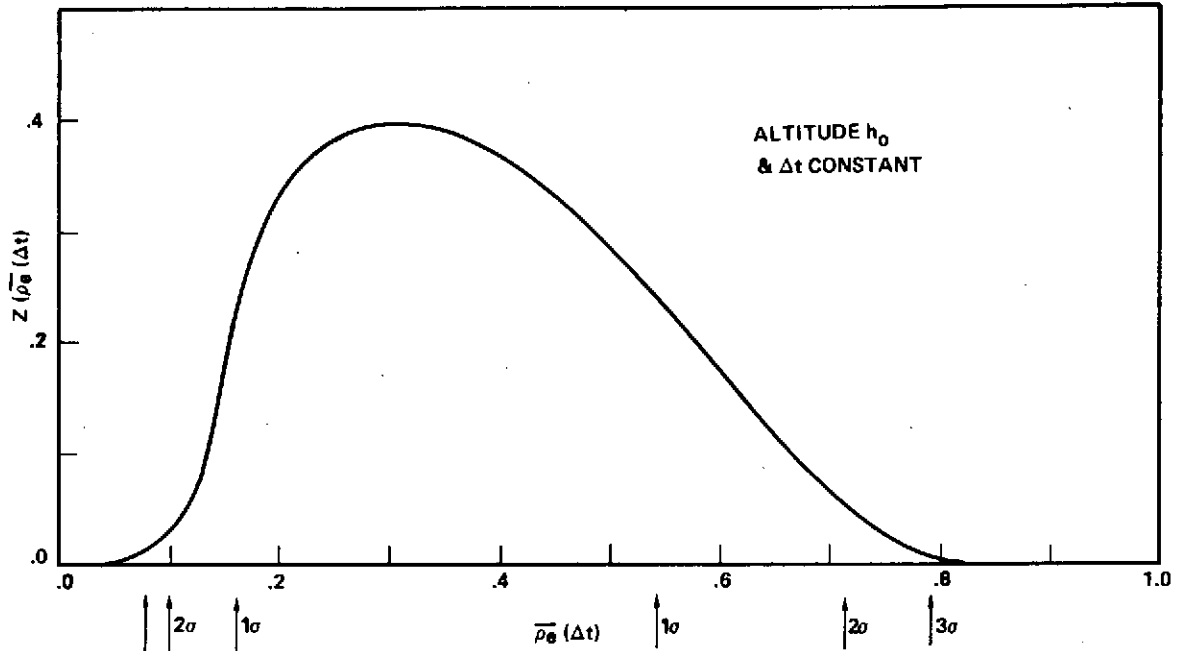
Figure 19. Probability distribution function for the effective
albedo at an altitude h_0 and a time increment Δt.

are used to curve fit $Z[\overline{\rho_e(\Delta t)}]$ to the function $g_0 \pm g_1 \exp[-k(\Delta t)]$ for 1σ, 2σ, 3σ values as a function of Δt. The results, with the present criteria values for comparison, are shown in Figure 20. The approach is not necessarily optimum, but it is a possible method of derivation of the appropriate criteria values, and the curves do indicate the physical behavior expected with a minimum effort.

Satellite Derivation

In an attempt to define the albedo probability distribution from satellite data, a simple procedure was developed to analyze Applications Technology Satellite (ATS) III photographs. An outline of the procedure is as follows:

1. The geographic surface features were assigned albedo values and a 2.0 by 2.0 deg grid was created.

2. Visual inspection of an ATS photograph led to assignment of cloud albedo in grid form.

TABLE — EQUATIONS FOR TIME AVERAGE EFFECTIVE ALBEDOS $\bar{\rho}_e$

	3 σ	2 σ	1 σ
$\bar{\rho}_{e_{max}}$	$.35 + .443e^{-1.0908 \Delta t}$	$.33 + .38e^{-1.2695 \Delta t}$	$.316 + .232e^{-1.3068 \Delta t}$
$\bar{\rho}_{e_{min}}$	$.25 - .17e^{-.6119 \Delta t}$	$.28 - .17e^{-.6536 \Delta t}$	$.284 - .121e^{-.9813 \Delta t}$

$$\bar{\rho}_e = \int_0^{\Delta t} \rho_e(t)dt / \Delta t$$

Figure 20.   The 1, 2, and 3 σ confidence levels for maximum and minimum time average effective albedo.

3. The two grids were merged.

4. A Lambertian earth is assumed and, hence, the sun angle was neglected.

5. Assuming a height and inclination, the position of the orbiting detector was calculated as a function of time.
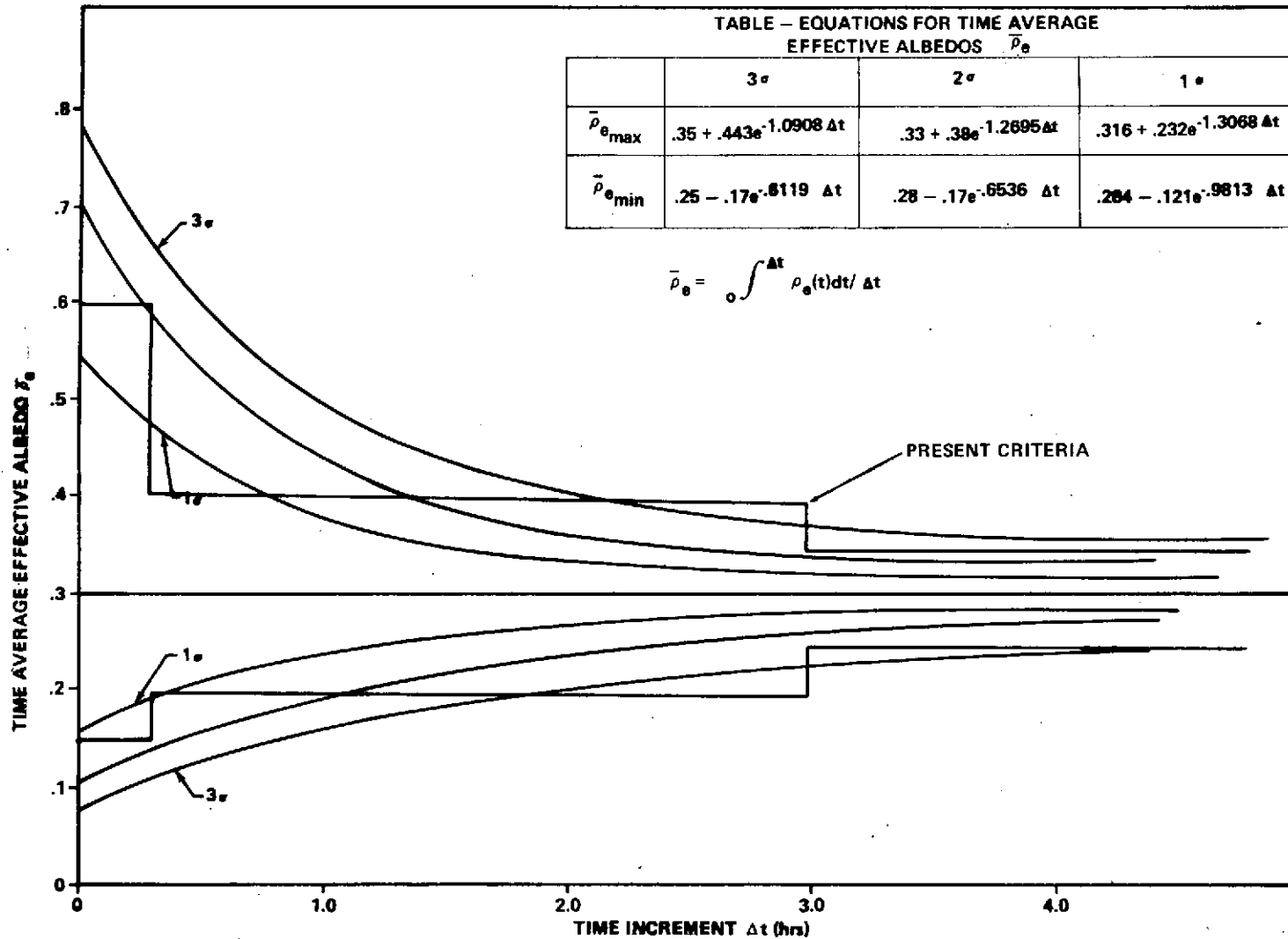
6. The time average effective albedos were calculated.

7. Finally, the 1σ, 2σ, 3σ values were determined.

A similar procedure for steps 1 through 4 was discussed by Bartman [2]; however, neither the TAEA nor the usefulness of the results to the thermal design engineer was discussed.

Figure 21 presents a portion of the cloud matrix between ±60 deg latitude and 0 to 70 deg longitude. The values of the albedo of the clouds were assumed according to the type and visual indications. Figure 22 presents the surface features where water was assumed to have an albedo of 0.10 and land one of 0.30. Several orbit paths are shown. The assumptions for the albedo of water and for underestimating the cloud cover lead to an accumulation of 0.10 values in the albedo distribution for the earth-atmosphere system. This distribution is shown in Figure 23.

For eight orbits and 400 points on the earth-atmosphere surface, Figure 24 shows the relative frequency of the calculated TAEA for $\Delta t = 0.5$, 5.3, 16.0, and 42.5. The orbit was assumed to have a 50-deg inclination and a 556-km altitude. The resulting 1σ and 3σ limits are given in Figure 25. The roughness of the calculation did not allow the actual 2σ and 3σ values to be determined. The 3σ given is the 100 percent probability limit. Figure 26 shows the same results except that the inclination is 18 deg. Because of the lower albedo values near the equator, the mean global average is lower. The general trend is, again, the same as from the transform results. The error bar on Figures 25 and 26 indicates the probable error of the data points given the assumed albedo matrices for the surface and cloud features. This is an example of the type of data that could be extracted from satellite data.

Satellite Data Study

The general procedure to determine the thermal design parameters from satellite data is as follows: Convert existing satellite data from selected orbits for which both instantaneous values of the earth thermal and albedo radiation can be obtained into data which can be easily handled. Use these data to
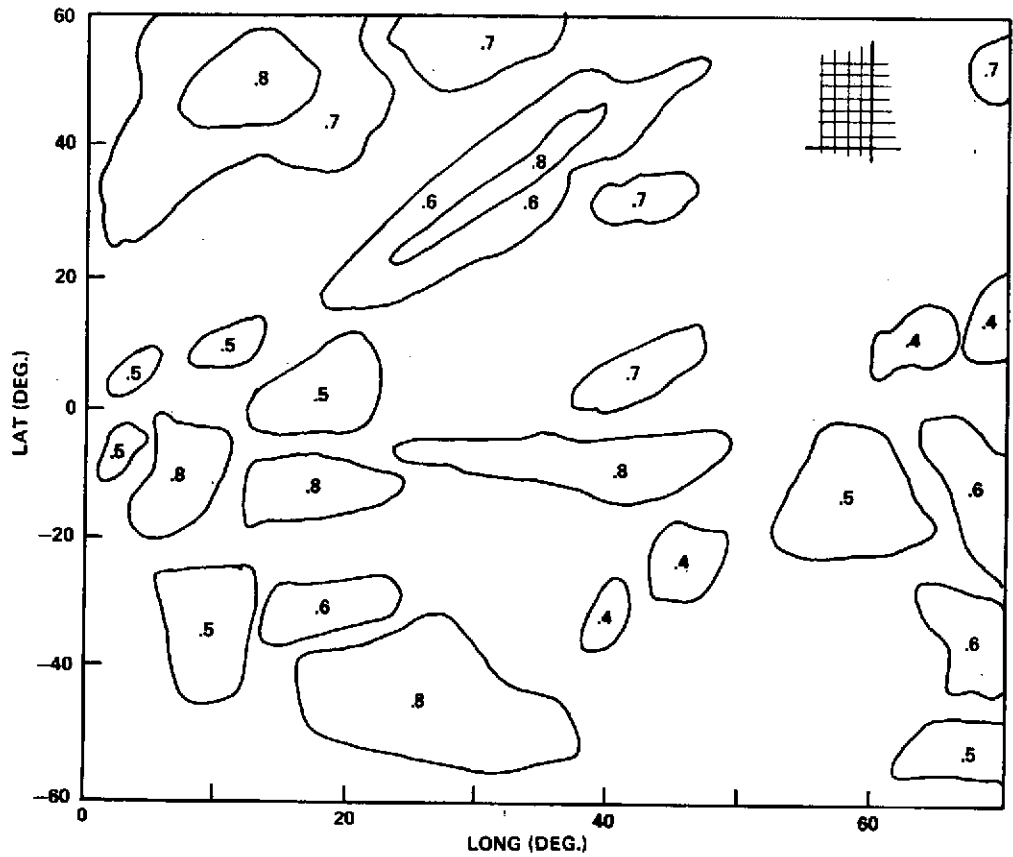
Figure 21. Cloud cover grid for the earth.
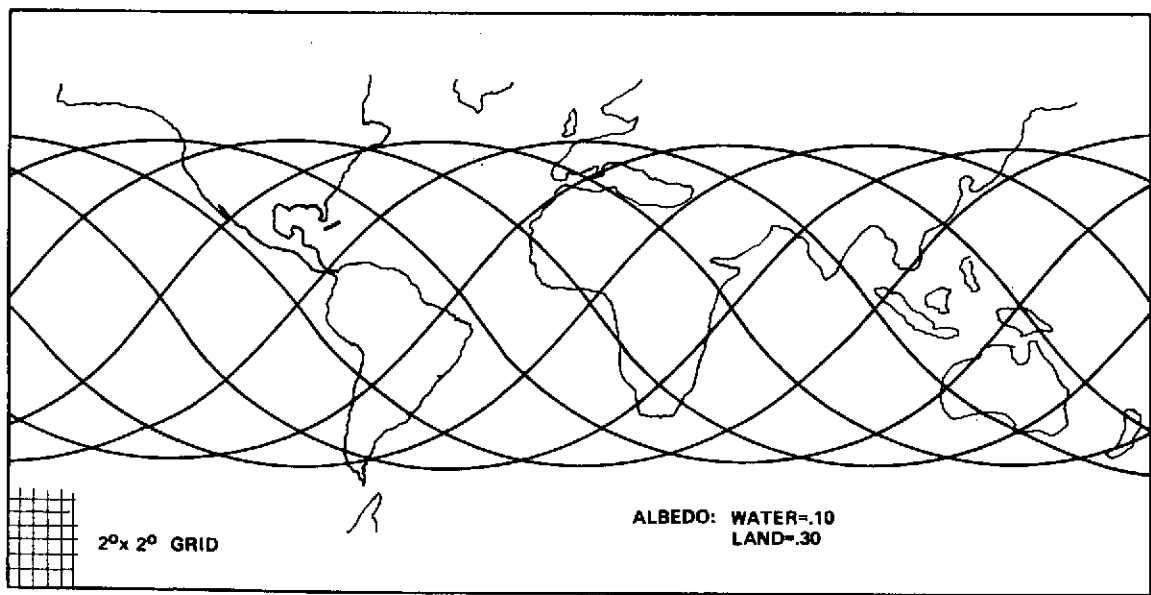
Figure 22. Surface grid for the earth.
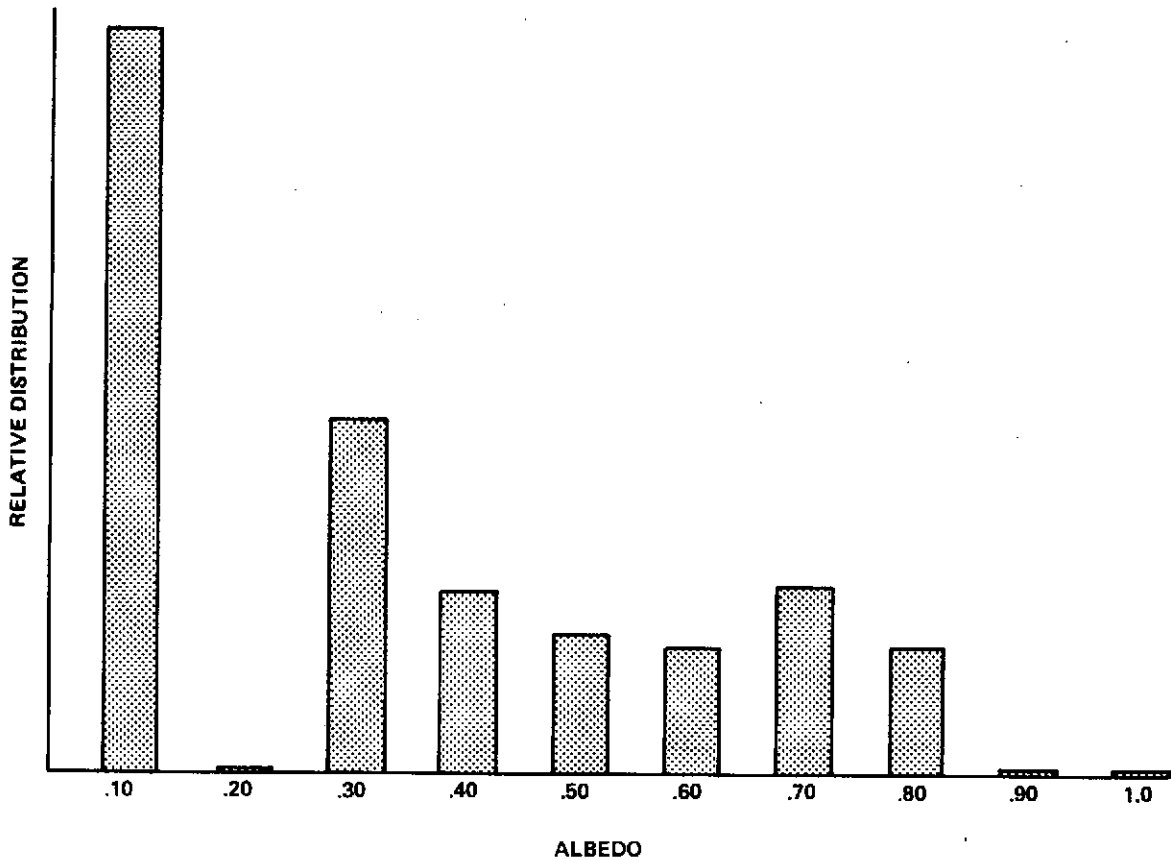
Figure 23. Albedo distribution for the earth-atmosphere surface.

calculate the instantaneous values which are summed over various time increments of consecutive parts of an orbit to obtain the time average effective value (TAEV). Determine the associated confidence levels by a statistical study of the different TAEV's. Analyze the accumulated data for the effects of orbit inclination, angle between orbital plane and earth-sun line, time of year, and orbital position. Evaluate the results and present them in a form that can be used for design purposes.

The second generation meteorological spacecrafts of the Nimbus series, specifically II and III, seem to provide sufficient data to deduce information on the time average effective values. The Nimbus spacecrafts carried radiometers which were always pointed directly toward the earth. The orbits were nearly circular at about 1100 km and were almost polar. The angle of inclination of approximately 80 deg provided an orbit which remained oriented along the earth-sun line (i.e., sun-synchronous).
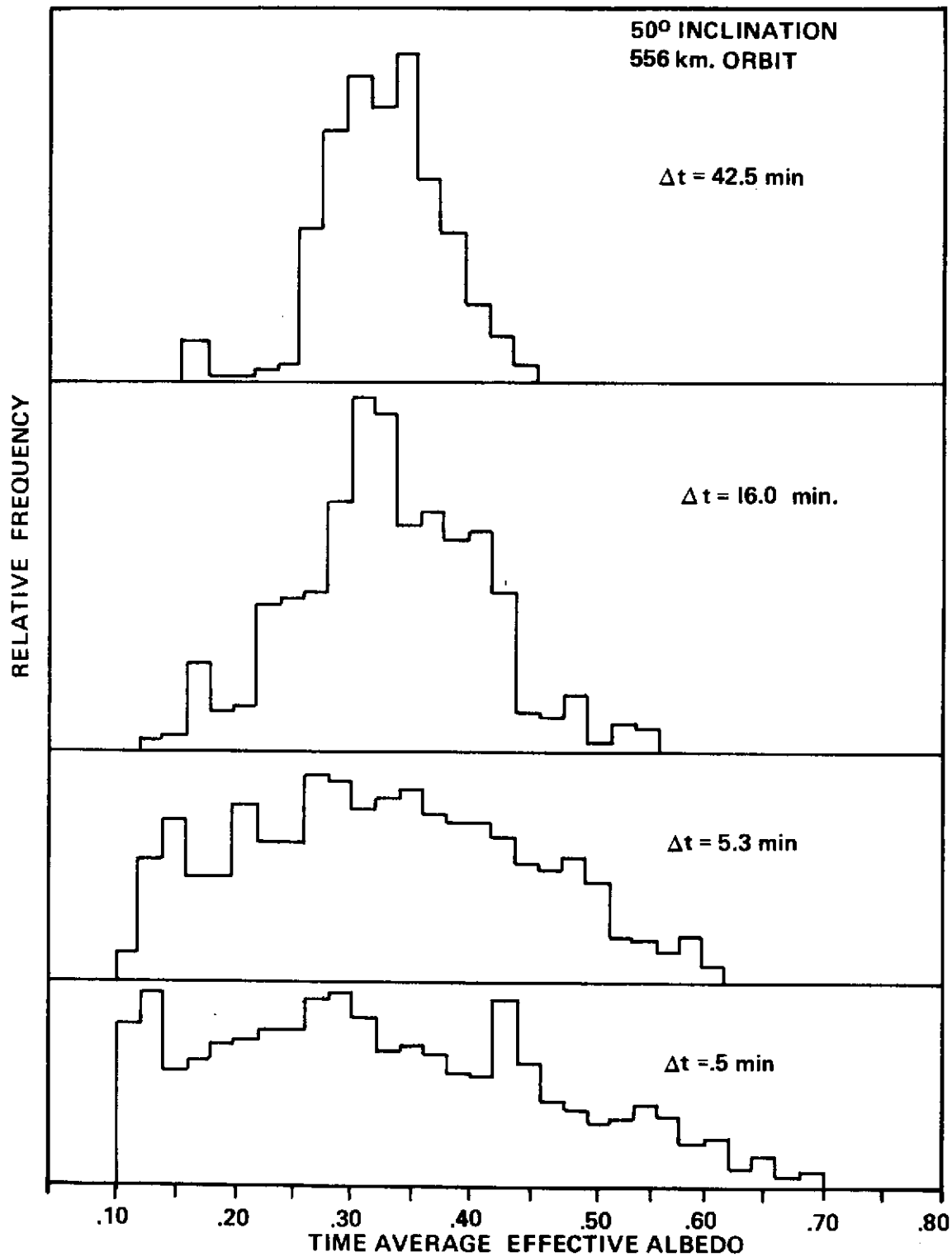
Figure 24. TAEA distribution for Δt = 42.5, 16.0, 5.3, and 0.5 minutes.
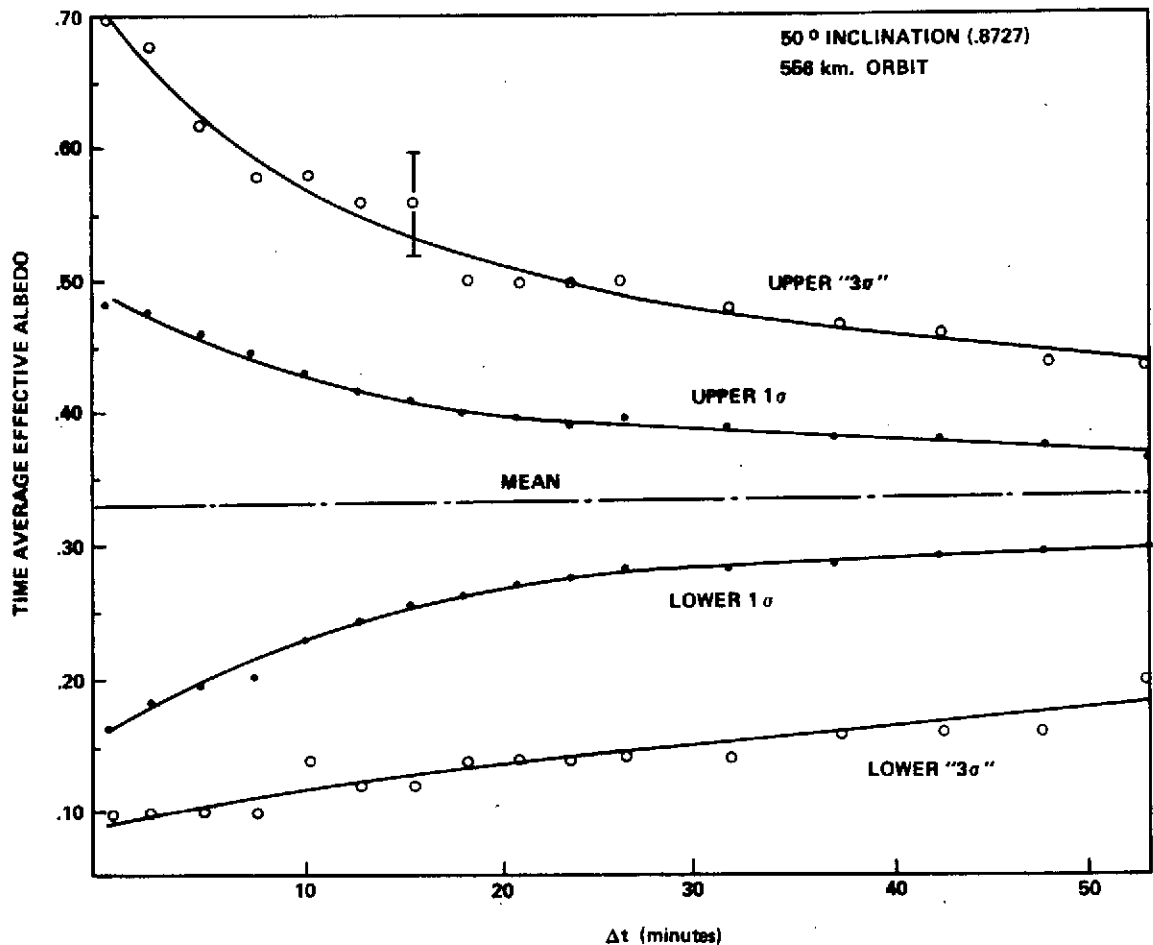
Figure 25. Time average effective albedo distribution for
50 deg inclination (8 orbit sum).

The radiometers and spectrometers on board provided data on the thermally emitted earth radiation and the reflected solar radiation emerging from the top of the atmosphere. The experiments on board Nimbus II and III which are of interest are listed in Table 5. The two channels of particular interest on Nimbus II are the medium resolution infrared radiometer (MRIR) 5 to 30 μm and 0. 2 to 4 μm channels. The 5 to 30 μm channel provides the radiance of 95 percent of the earth thermal radiation, while the 0. 2 to 4 μm channel provides the radiance values of 99 percent of the solar reflected radiation. Because the data of the MRIR on Nimbus II did not provide complete full-earth coverage and the instrument operated only 3 months, the desired thermal design parameters cannot be completely recovered from the data. The data of Nimbus III should be employed for better statistical results.
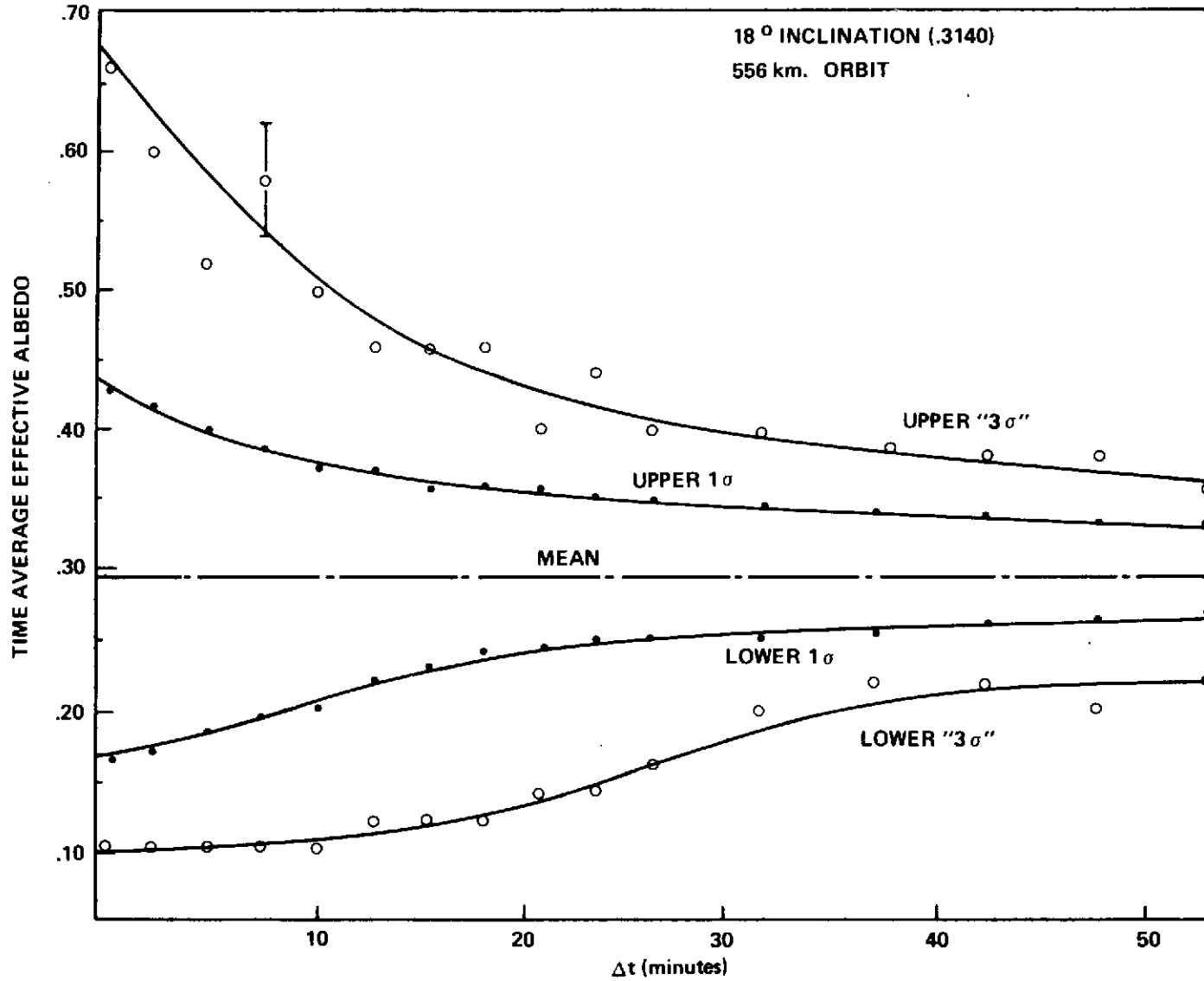
Figure 26. Time average effective albedo distribution for 18 deg inclination (12 orbit sum).

TABLE 5. NIMBUS SPACECRAFT SYSTEM

	Nimbus II	Nimbus III
Activities	May 15, 1966, launch May 22, 1966, operational July 26, 1966, 15 percent reduction of HRIR[a] data July 29, 1966, MRIR[b] data lost Nov. 15, 1966, HRIR data lost	Apr. 14, 1969, launch Apr. 22, 1969, operational July 22, 1969, IRIS[c] data lost Aug. 12, 1969, noisy HRIR data Aug. 28, 1969, MRIR[c] data reduced Oct. 1-15, 1969, full coverage of earth by MRIR Jan. 31, 1970, MRIR pictures terminated Sept. 25, 1970, altitude control failure
Orbital Data	Height — 1179 by 1095 km orbit Inclination — 79.689 deg retrograde orbit Period — 108 min Sun-synchronous	Height — 1101 km Inclination — 80.1 deg retrograde Period — 107 min Sun-synchronous
Experiments of Interest	1. MRIR Spectral Bands (μm) (50 km resolution) 6.4-6.9 atmosphere H_2O and cirrus cloud mapping 10-11 surface and cloud top temperatures	1. MRIR Spectral Bands (μm) (50 km resolution) 6.5-7.0 atmospheric H_2O and cirrus cloud mapping 20-23 atmospheric H_2O and cirrus cloud mapping

TABLE 5. (Concluded)

	Nimbus II	Nimbus III

Experiments of Interest (Concluded)	14-16 stratosphere temperatures
	5-30 total thermal radiation and heat budget
	0. 2-4 daytime cloud mapping, albedo and heat budget
	
	2. HRIR Spectral Bands (μm) (10 km resolution)
	    3. 5-4. 1 nighttime cloud coverage
		10-11 surface and cloud top temperatures
		14. 5-15. 5 stratospheric temperatures
		0. 2-4. 0 daytime cloud mapping, albedo, and heat budget
		
		2. HRIR Spectral Band (μm) (10 km resolution)
		    3. 4-4. 2 nighttime surface and cloud cloud top temperatures and cloud mapping
		    0. 7-1. 3 daytime cloud mapping
		
		3. IRIS Spectral Band 5-20 μm (150 km resolution)
		    Atmospheric temperature profile, O_3, water vapor, and surface temperature

a. HRIR — High resolution infrared radiometer
b. MRIR — Medium resolution infrared radiometer
c. IRIS — Infrared Interferometer Spectrometer

44

Nimbus III did not have the 5 to $30\,\mu$m channel which provides direct information on the total earth-emitted thermal radiation. However, one can correlate the HRIR data of Nimbus II and III and the IRIS data of Nimbus III with the data from the MRIR's of both spacecraft to provide data for a procedure to obtain satisfactory thermal data from Nimbus III. The Nimbus III data provide a longer time of observation.

A program to determine thermal environment parameters from satellite data is under study. The program will employ the Nimbus II and Nimbus III spacecraft experiment data obtained by the MRIR, the HRIR, and the IRIS experiments.

Computer programs using the Nimbus data in digital format are to be developed to allow a statistical study of the data to determine the following near-earth thermal design parameter objectives for the earth's thermal and reflected solar radiation:

1. Objective 1. The probability distribution function of the time average effective values and the 1, 2, and 3σ confidence limits (i.e., the 68.3, 95.4, and 99.7 percent confidence level limits) for various orbital time integration intervals Δt's.

2. Objective 2. Global average value for the data maps processed under objective 1. The global average value for each map generated under objective 1.

3. Objective 3. The effect of the variation of the orbit height and the orbital time integration interval and their interrelationship on the TAEV sigma values. The study will be performed by calculating the TAEV sigma value limits for various orbital heights.

4. Objective 4. The relation of the earth-emitted thermal radiation and the albedo values and their sigma level confidence limits for simultaneous data will be determined by interrelating the 5 to 30 and 0.2 to 4 μm channels of the MRIR on Nimbus II to allow the determination of the procedures to calculate the total thermal inputs into a spacecraft of both albedo and earth thermal radiation. The interdependence will be presented to allow the design engineer to calculate the root-mean-square averages of the heat input and specify these procedures.

The interdependence will be in a form such that given a time average effective albedo for Δt, both the high and low values of the expected earth thermal radiation can be obtained for 1, 2, and 3σ confidence levels [i.e., for a time average effective albedo $\overline{\rho_e(\Delta t)}$, the earth thermal radiation has a $n\sigma$ confidence of being below $b_1 + b_2 \exp(-b_3\Delta t)$].

5. Objective 5. The distribution of the rate of change of the TAEV's will be determined for the various orbital time integration limits.

6. Objective 6. The relation of the sun-earth-spacecraft position (phase relation) on the time average effective albedo values will be determined for phase angles from 0 to 90 deg. This will give the dependence of the directional reflectance of the albedo on the solar zenith angle.

7. Objective 7. The effect of inclination on the sigma value confidence limits will be determined.

The Nimbus II MRIR and HRIR data will be analyzed for various numbers of orbits, and the Nimbus III MRIR, HRIR, and IRIS data will be analyzed to provide the correlation between the four thermal radiation channels of 6.5 to 7.0, 20 to 23, 10 to 11, and 14.5 to 15.5 of Nimbus III MRIR and HRIR channels. The correlation will provide a procedure to determine the total earth thermal radiation from Nimbus III data.

Using the above correlation, the Nimbus II and III MRIR data will be transformed by integrating the data over areas of 160 km by 160 km into grid maps for the earth-emitted thermal radiation and albedo radiation levels. A grid map is a matrix of elements for which the location in the matrix is given by earth latitude and longitude and the value of the matrix element is the average value of the Nimbus data over an earth-atmosphere area of approximately 160 km by 160 km. Each grid map is representative of the values obtained during a 24-hour period over the entire earth. Conversion for geometry and spectral band approximations are to be given. The earth is assumed to be a Lambert reflector for the solar radiation. Each grid map will be representative of the Nimbus data obtained for a 24-hour period covering the entire earth. The days considered will be separated in time as equally as possible over a typical year or portions allowed by the lifetime of the experiments. For portions of the earth not covered by the Nimbus data during a specific day, appropriate interpolation values will be estimated using data obtained on consecutive days or adjacent areas. These grid maps will model the earth albedo and thermal radiation for the various days.

The constructed grid maps (i.e., a matrix of albedo and thermal values of the earth-atmosphere system) will be employed to calculate the time average effective values of both the albedo and earth thermal radiation. The orbital node angle will be randomly distributed to average out any effects which it might introduce. The TAEV's will be calculated using a set of orbits covering the entire modeled earth per grid map. The second half of the consecutive orbits should be displaced by one-half of the longitude displacement for one orbit.

For $\Delta t = 0$ the TAEV will be calculated at 30-sec intervals for determining the other TAEV values and the effects of height, inclination, and orbital motion.

The sigma level confidence limits will be calculated from the distribution of the TAEV. The upper and lower confidence level limits of 68.3, 95.4, and 99.7 percent for each orbital time integration interval given in objective 1 will be determined.

The results of the confidence level limits study will be presented in a tabular form giving the earth thermal radiation and albedo values at which the three confidence level upper and lower limits lie for each of the 100 days and the values for the average of the results for 3-month periods. A parameterized function of $C_1 + C_2^{(u,1)} \exp[-C_3^{(u,1)} \Delta t]$, where C_1, C_2, and C_3 are parameters and $(u, 1)$ specify the upper or lower limit parameter, will be fitted to each confidence level for the values of Δt. The display of the result will be in a form similar to Figure 20.

The results of the global average per grid map and the total global average will be tabulated for the earth's thermal and albedo values obtained from the study.

The effect of the orbital height on the effective time integration limit will be given in a parameterized form so that, given the sigma level, confidence limits for any height can be determined from the results of a specific height. The parameters can be given in the form:

$$a_1 = \frac{\partial}{\partial h} \left\{ Z[\overline{\rho_e(\Delta t)}] \right\}_{\Delta t}$$

$$a_2 = \frac{\partial}{\partial h} \left\{ Z[\overline{\rho_e(\Delta t)}] \right\}_{\Delta t}$$

$$a_3 = \frac{\partial}{\partial \Delta t} \left\{ Z[\overline{\rho_e(\Delta t)}] \right\}_{h=h_0}$$

$$a_4 = \frac{\partial}{\partial \Delta t} \left\{ Z[\overline{\rho_e(\Delta t)}] \right\}_{h=h_0} .$$

These parameters will allow an increased height in orbit to be related to an increase in the time increment.

Since the bidirectional effects have been averaged out and the earth is assumed to be a Lambertian reflector, the effect of solar position is to be included. The limb darkening effects for thermal radiation will also be included.

The rate at which $\overline{\rho_e(\Delta t)}$ and $\overline{IR(\Delta t)}$ can change with respect to time is important in creating various theoretical heat load inputs which are allowed under the given parameters. These distributions will be presented in the results.

The relation between the thermal and albedo values will be included. This is a result of the fact that cloud cover increases the albedo but decreases the IR received because the radiating layer seen is higher in the atmosphere. This will affect the root-mean-square procedures employed by the designer.

The specular ocean reflections will be included as singularities at the appropriate conditions.

APPLICATION PROCEDURES

In the past, the thermal design engineer has dealt mainly with slow response systems and systems which could be overdesigned, but now there are many thermal design applications in which the tolerances cause the uncertainty in the thermal evaluation to approach significant magnitude. For large-scale environmental control systems in spacecrafts, a 5 to 8° C (10 to 15° F) uncertainty in the albedo and IR effects has significant impact.

Figure 27 shows the temperature of a shell versus orbital position with the surface density as a parameter. The thickness Δx necessary for a surface density ρ_s is given by:

$$\rho_s = \frac{\rho_v V}{S} = \frac{\rho_v \left[\frac{4}{3} \pi r^3 - \frac{4}{3} \pi (r - \Delta x)^3 \right]}{4 \pi r^2} \quad . \tag{32}$$

Table 6 gives the thickness for a 1-meter radius shell for aluminum and gold. It is seen that a small surface density corresponds to thin elements such as detectors and solar cell elements. As shown in Figure 27, as the mass of the surface increases, the temperature excursion in orbit decreases [15]. Also, as the surface density increases, the calculated mean temperature increases to
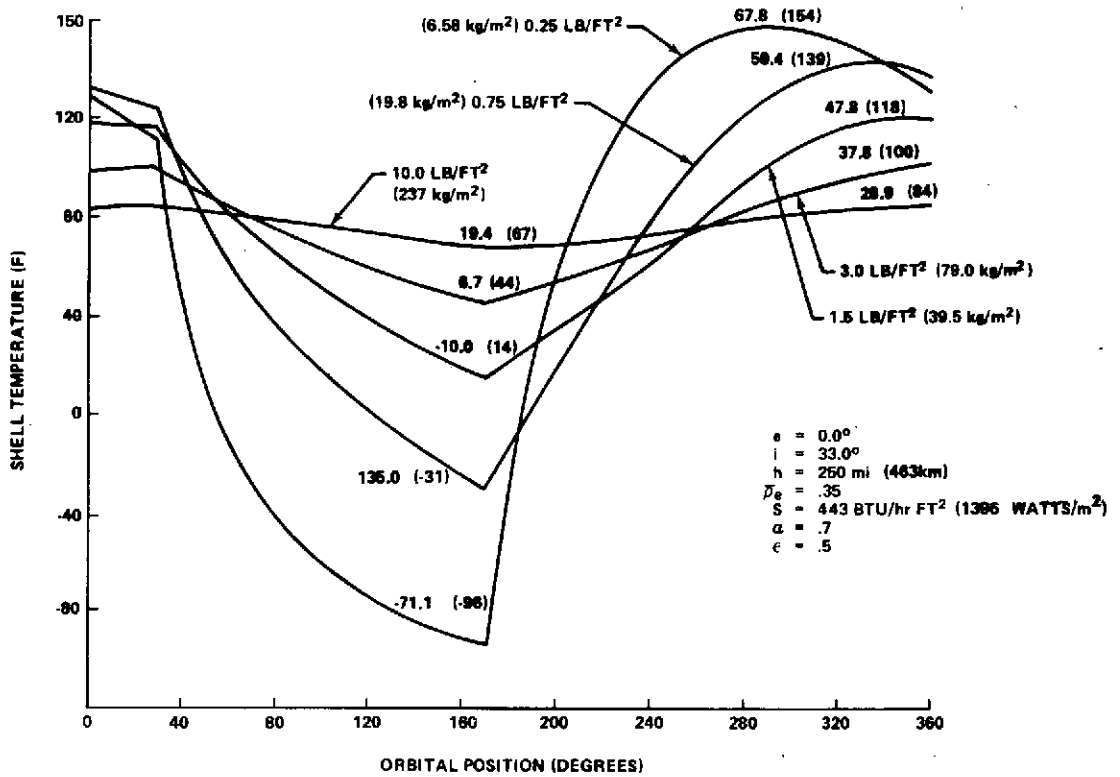
Figure 27. Temperature history of an orbiting shell [15].

TABLE 6. SHELL THICKNESS AND DENSITIES

ρ_s (lb/ft^2)	ρ_s (kg/m^2)	$\Delta x - Al$ (ρ_{vAl} = 2700 kg/m^3)	$\Delta x - Ag$ (ρ_{vAg} = 19 300 kg/m^3)
10.0	237.0	36.7 cm	5.1 cm
3.0	79.0	12.2	1.7
1.5	39.5	6.1	0.85
0.75	19.8	3.0	0.43
0.25	6.58	1.0	0.14

49

the limiting temperature which is given by

$$T_{\text{mean limit}} = \sqrt[4]{\frac{T^4_{\text{max}} + T^4_{\text{min}}}{2}} \quad . \tag{33}$$

Table 7 gives the mean, maximum, and minimum temperatures shown in Figure 27 [15].

TABLE 7. MINIMUM AND MAXIMUM TEMPERATURES FOR SHELL

ρ_s (kg/m²)	Mean [°C (°F)]	Max [°C (°F)]	Min [°C (°F)]	$\sqrt[4]{(T^4_{\text{min}} + T^4_{\text{max}})/2}$ [°C (°F)]
6.58	6.7 (44)	67.8 (154)	-71.1 (-96)	22.0 (72)
19.8	16.7 (62)	59.4 (139)	-35.0 (-31)	23.3 (74)
39.5	19.4 (67)	47.8 (118)	-10.0 (14)	23.1 (74)
79.0	21.7 (71)	37.8 (100)	6.7 (44)	23.5 (74)
237.0	22.2 (72)	28.9 (84)	19.4 (67)	24.3 (76)

The reaction of a system to the environment depends on the environment and on the design of the system. The albedo and IR criteria should be given so that they are independent of the system but are capable of being combined with the parameters of the system to give its thermal history. The significance of the time average effective albedo can be seen in this context by introducing a function called the "thermal time constant of the system." The temperature is assumed to be of the form

$$T = T_0 e^{-t/\tau} \tag{34}$$

where τ is the thermal time constant [16]. If it is near equilibrium, the thermal time constant can be defined as

$$\tau = \frac{mc_p}{16A\sigma\epsilon_{IR}T_0^3} \quad , \tag{35}$$

then

$$\tau = \rho_s \, 400 \text{ sec m}^2/\text{kg} \quad . \tag{36}$$

Hence, for the shells considered earlier,

τ = 26.3 hr ρ_s = 237 kg/m^2

 = 8.78   = 79

 = 4.39   = 39.5

 = 2.11   = 19.2

 = 0.7311   = 6.58

For the lowest surface densities, the values of τ are approximately equal to the time necessary for a half revolution. Hence, the time average effective albedo for $\Delta t \simeq 30$ min would be of particular importance. For a shell with the following parameters:

e = 0.0

i = 33 deg

h = 250 n. mi. (463 km)

ρ_s = 1.5 lb/ft^2 (39.5 kg/m^2)

S = 1396 W/m^2 (443 BTU/hr/ft^2)

α = 1.0

ϵ = 1.0

α/ϵ = 1.0   ,

the minimum and maximum values of the temperature for various albedos are given in Table 8.

TABLE 8. MINIMUM AND MAXIMUM TEMPERATURES FOR
VARIOUS ALBEDOS

Albedo	Maximum Temperature [°C (°F)]	Minimum Temperature [°C (°F)]
0.20	29.4 (85)	-35.6 (-32)
0.35	33.9 (93)	-38.9 (-38)
0.50	37.8 (100)	-42.2 (-44)
0.80	47.8 (118)	-49.4 (-57)

The probability function for the time average effective albedo would indicate the chance of seeing albedos such as those in Table 8, or, equivalently, the chance of having those maximum and minimum temperatures. For a particular daytime pass, the instantaneous average albedo can be any value between the limits given by the probability function of TAEA.

A question that arises is, how long can a specific value $\overline{\rho_e(t, \Delta t = 0)}*$ be seen assuming a certain $K\sigma$ value (K = 1, 2, 3)? The period of time is just the value of Δt which gives

$$\overline{\rho_e(t, \Delta t)} = \overline{\rho_e(t, \Delta t = 0)}* \quad . \tag{37}$$

For example, if K = 3 and $\overline{\rho_e(t, \Delta t = 90)} = 0.35$, then one could have $\overline{\rho_e(t, \Delta t = 45)} = 0.474$ for 45 min and $\overline{\rho_e(t, \Delta t = 45)} = 0.226$ for 45 min as long as these values are within the 3σ limits for the distribution. Furthermore, the value during 15-min intervals for $\overline{\rho_e(t, \Delta t = 15)}$ could flip-flop between 0.508 and 0.192. This example represents a hot case for 3σ since $\overline{\rho_e(t, \infty)} = 0.35$. Figure 28 represents various ways that such a hot case for a pass could be introduced into a thermal design program for thermal analysis. Each segment is such that if extended it would give an 0.35 average over a period of time.
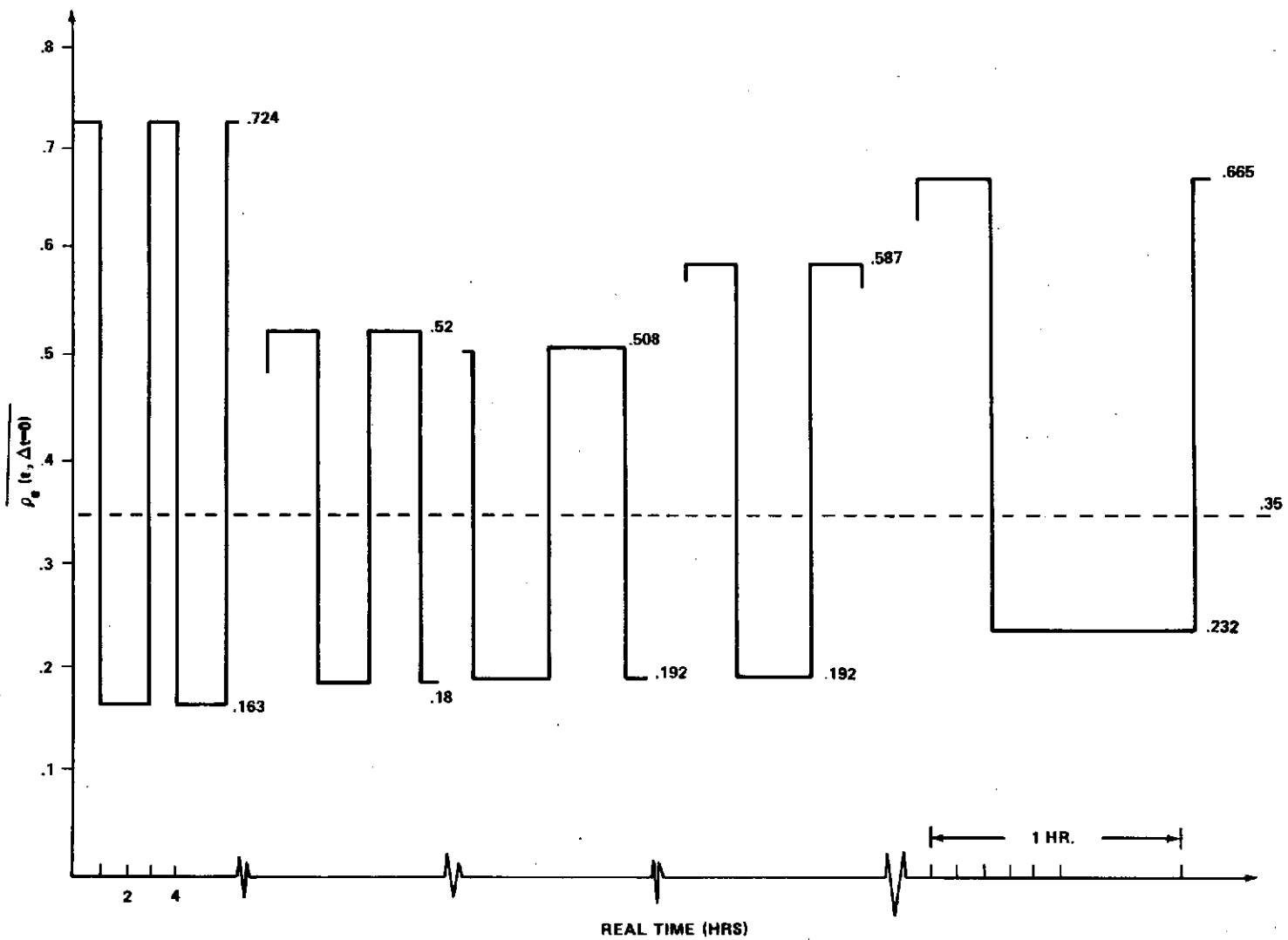
Figure 28. The 3σ hot case: Examples of time histories generation of $\overline{\rho_e(t, \Delta t = 0)}$.

The instantaneous change is not necessary. A finite slope up to a maximum of 1.6×10^{-3} sec could have been introduced for a 463-km orbit.
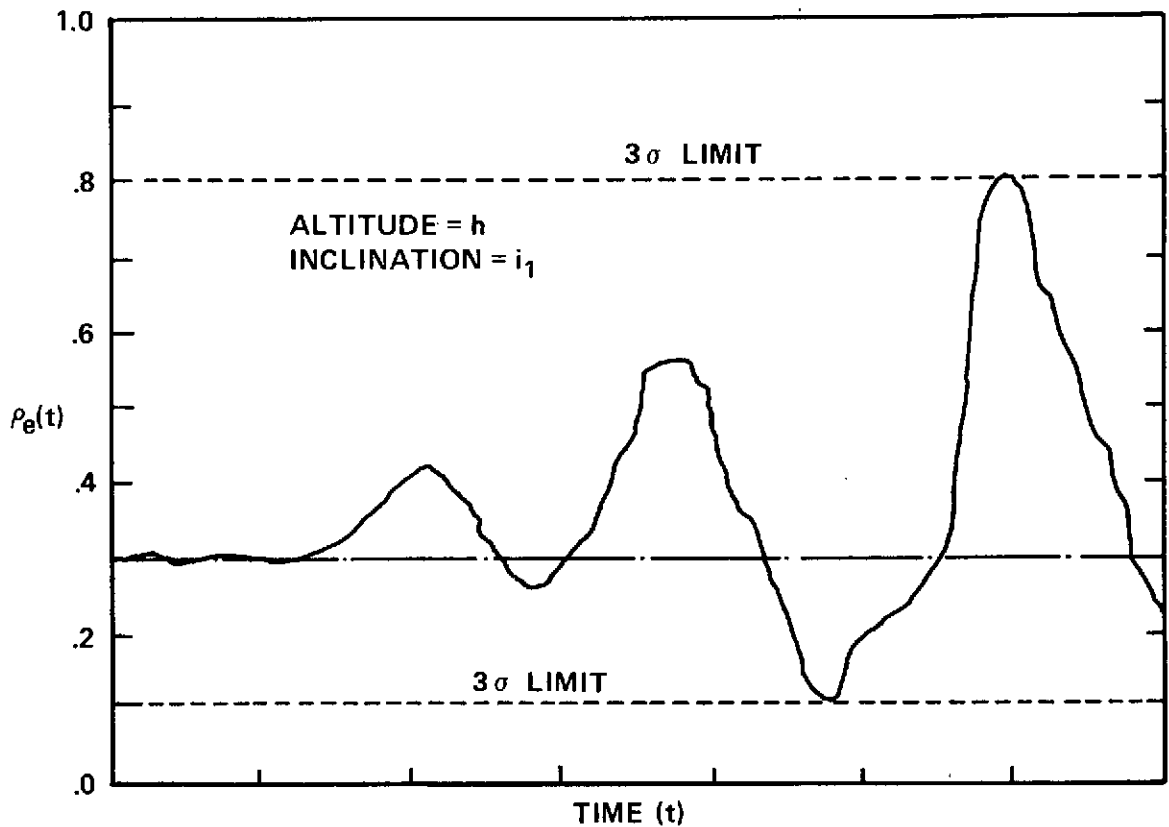
The general limitations in parameterized form for the time history of the albedo are summarized in Figure 29. In this figure an example of a time history is given which considers those limitations. In generating criteria, various "hot" and "cold" examples of time histories can be generated as guidelines for the thermal designer. The albedo, though, must be correlated with the thermal radiation. The parameter of the time average albedo could be displayed as in Table 9. Alternately, since for a specified σ limit

$$\overline{\rho_e(t, \Delta t)}\bigg|_{Z=K\sigma} = \overline{\rho_e(t, \Delta t = \infty)} + a_i^{(u,1)} e^{-b_i^{(u,1)}\Delta t} e^{-c_i^{(u,1)}h/R} \, ,$$

$$(38)$$

where $(u, 1)$ are the upper and lower limits and a^1 and a^u have opposite signs, the values for a_i, b_i, c_i could be tabulated for season, inclination, and sigma limits. Similar results would be obtained for the thermal value. Then the thermal designer, knowing the system and expected orbit, could find the albedo and IR values and range that would be encountered by the system.

CONCLUSION

In summary, the variation of the earth thermal and albedo radiation received by a near-earth orbiting space vehicle or space payload as a result of temporal variations of earth-atmosphere has been discussed. The term "time average effective value" was introduced and defined as the average of the effective value of the albedo or thermal radiation affecting a thermal system in orbit over a given orbital segment defined by an increment in time. These are the important values to the thermal designer. The values are independent of the spacecraft and dependent only on the character of the earth-atmosphere system. The time average effective values have a probability distribution that is dependent on the time increment. A statistical study of current satellite data can give this probability distribution. With this distribution, the thermal designer can define confidence levels on predicted temperature ranges which are compatible with engineering models for use in design, failure probabilities, and spacecraft cost estimates.

54

LIMITATIONS OF $\bar{p}_e(t)$ (HENCE INCLUDES $p_e(t) = \bar{p}_e(\Delta t = o)$),
FOR 3σ LIMIT WORST CASE:

(1) $\left| \dfrac{d\,\bar{p}_e}{d\,t} \right|_{\text{MAXIMUM}} < C_0 + C_{,e}^{-k\Delta h}$

(2) $\bar{p}_e(\Delta t) = \displaystyle\int_0^{\Delta t} p_e(t)\, dt/\Delta t \begin{cases} < A_1 + a_1\, e^{-K_1\,\Delta t} \\ > A_2 - a_2\, e^{-K_2\,\Delta t} \end{cases}$

(3) $\bar{p}_e \; (\Delta t = o) = p_e(t) = \begin{cases} < .793 \\ > .080 \end{cases}$

Figure 29. The limitations on the TAEA and an example of using these limitations to form a time history of the TAEA.

TABLE 9. TIME AVERAGE EFFECTIVE ALBEDO

Sphere: Δt = 30 min Season = July Inclination = 35 deg			
Altitude (km)	1	2	3
500	$0.30^{+0.13}_{-0.10}$	$0.30^{+0.22}_{-0.17}$	$0.30^{+0.33}_{-0.19}$
750	$0.30^{+0.12}_{-0.09}$	$0.30^{+0.20}_{-0.16}$	$0.30^{+0.25}_{-0.18}$
1000	$0.30^{+0.11}_{-0.08}$	$0.30^{+0.19}_{-0.115}$	$0.30^{+0.23}_{-0.14}$

The parameters for the thermal design engineer in the area of thermal and albedo radiation are summarized below:

1. Probability distribution functions for the time average effective albedo and thermal radiation and the time rate of change distributions.

2. The global albedo and thermal radiation averages.

3. The functional dependence of the probability distribution functions of the variation of height, time increment, and solar zenith angle.

4. The correlation function between the thermal infrared and albedo radiation.

5. The separation of the radiation into specular and diffuse components, and surface and atmospheric components.

Before the particular parameter studies can be undertaken, the probability distribution function for the time average effective values must be determined in a meaningful manner. It is proposed that these functions are highly desirable and necessary for future spacecraft thermal design studies.

REFERENCES

1. Smith, R. E.: Space and Planetary Environment Criteria Guidelines for use in Space Vehicle Development. NASA TM X-64627, 1971 Revision, Nov. 15, 1971, pp. 1-11, 2-30 through 2-33.

2. Bartman, F. L.: The Reflectance and Scattering of Solar Radiation by the Earth. University of Michigan, NASA CR-83954, 1967.

3. Meyer-Arendt, R.: Radiometry and Photometry: Units and Conversion Factors. Applied Optics, vol. 7, 1968, pp. 2081-2084.

4. Christensen, E. M.: Radiation Geometric Factors Between Planets and Space Vehicles. AF 18(600)-1775, General Dynamics, 1962.

5. Wolfe, W. L., Ed.: Handbook of Infrared Technology. U. S. Government Printing Office, 1965.

6. Earth Albedo and Emitted Radiation, NASA Space Vehicle Design Criteria (Environment). NASA SP-8067, July 1971.

7. Snoddy, W. C.: Irradiation Above the Atmosphere Due to Rayleigh Scattering and Diffuse Terrestrial Reflections. AIAA Paper No. 65-666, AIAA Thermophysics Specialist Conference, Monterey, California, Sept. 13-15, 1965.

8. Jones, R. W.: Factors Affecting the Near-Earth Thermal Environment. SMSD-SSL-1129, Teledyne Brown Engineering, Huntsville, Ala., Apr. 1970.

9. Barnes, J. C. and Chang, D.: Accurate Cloud Cover Determination and Its Effects on Albedo Computations. Report No. 9G53-12, Allied Research Associates, Inc., Geophysics and Aerospace Division, Oct. 1968.

10. Whitehill, L. P.: Survey on Earth Albedo. Tech. Rept. No. 1966-53, Lincoln Laboratory, MIT, Oct. 11, 1966.

11. Pearson, B. D., Jr. and Neal, C. B.: Albedo and Earth-Radiation Measurements from OSO-II. Paper 67-330, AIAA Thermophysics Specialist Conference, New Orleans, La., Apr. 17-20, 1967.

REFERENCES (Concluded)

12. Linton, R.C.: Earth Albedo Studies Using Pegasus Thermal Data. Prog. in Astron. and Aeron., vol. 20, 1967, pp. 475-490.

13. Raschke, E.: The Radiation Balance of the Earth-Atmosphere System from Radiation Measurements of the Nimbus II Meteorological Satellite. NASA TN D-4589, July 1968.

14. Kornfield, J. and Hasler, A.F.: A Photographic Summary of the Earth's Cloud Cover for the Year 1967. J. of App. Meteor., vol. 8, no. 4, Aug. 1969, pp. 687-700.

15. Stevenson, J.A.: Radiation Heat Transfer Analysis for Space Vehicles. ASD Technical Report 61-119, Space and Information Systems Division, North American Aviation, Inc., Wright-Patterson Air Force Base, Ohio, Dec. 1961.

16. Goldman, D.T. and Singer, S.F.: Studies of a Minimum Orbital Unmanned Satellite of the Earth (MOUSE), Part III Radiation and Temperature. Astronaut. Acta., vol. III, no. 2, 1957, pp. 110-129.
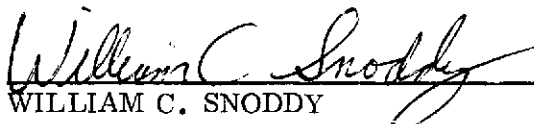
APPROVAL

THE DEFINITION AND SPECIFICATION OF THE NEAR-EARTH ENVIRONMENTAL CRITERIA FOR SPACECRAFT THERMAL DESIGN

By G. A. Gary and P. D. Craven

The information in this report has been reviewed for security classi-fication. Review of any information concerning Department of Defense or Atomic Energy Commission programs has been made by the MSFC Security Classification Officer. This report, in its entirety, has been determined to be unclassified.

This document has also been reviewed and approved for technical accuracy.

WILLIAM C. SNODDY
Chief, Astronomy and Solid State Physics Division

CHARLES A. LUNDQUIST
Director, Space Sciences Laboratory

DISTRIBUTION

INTERNAL

DA01
Dr. Lucas

DS30
Dr. Stuhlinger

ES01
Dr. Lundquist
Mrs. Tingle (5)

ES31
Dr. Naumann

ES21
Dr. Decher

ES11
Mr. Snoddy
Mr. Jones

ES12
Mr. Arnett

ES14
Mr. Miller
Dr. Gary (15)
Mr. Craven (15)

ES41
Mr. Vaughan

CC01
Mr. Wofford

AS61 (2)

AS61-L (8)

AT01 (6)

EXTERNAL

Scientific and Technical Information
  Facility (25)
P. O. Box 33
College Park, Maryland 20740
Attn: NASA Representative (S-AK/RKT)

Joel M. Dash
P. O. Box 8555
General Electric Company
Valley Forge Space Center
Philadelphia, PA 19101

Thomas H. Vonder Haar
Dept. of Atmospheric Science
Colorado State University
Fort Collins, CO 80521

R. L. Mancuso
Stanford Research Institute
333 Ravenswood Ave.
Menlo Park, CA 94025

Jaun K. Lovin
Lockheed Missiles & Space Co., Inc.
Huntsville Research & Engineering Center
4800 Bradford Drive
Huntsville, AL 35807

James C. Barnes
Environmental Research & Technology, Inc.
429 Marrett Road
Lexington, MA 02173

F. L. Bartman
College of Engineering
Dept. of Aerospace Engineering
High Altitude Engineering Laboratory
University of Michigan
Ann Arbor, MI 48104